Generation of negative skin friction and drag load in near-offshore pile foundations: A numerical study addressing pile installation effects

Michael Conrad Koch[a], Bhupendra Chand[b], Mousumi Mukherjee[b *], Arindam Dey[c]

[a]*Research School of Earth Sciences, Australian National University, Australia*
[b]*School of Civil and Environmental Engineering, Indian Institute of Technology Mandi, HP, India*
[c]*Department of Civil Engineering, Indian Institute of Technology Guwahati, Assam, India*
[*] *Corresponding Author, E-mail: mousumi@iitmandi.ac.in, mousumi.ju06@gmail.com*

ABSTRACT

Offshore and near-offshore infrastructures are primarily supported by pile foundations for transferring the super-structure load to the bearing stratum while bypassing the overlying soft consolidating medium. Apart from the characteristics of the surrounding consolidating soil medium, pile installation process can also significantly influence the development of negative skin friction on the installed piles for such applications. The present study elucidates the evolution of negative skin friction on both in-place and jacked pile with the aid of an updated Lagrangian-based 2D-axisymmetric finite-element simulation framework. A particular emphasis is given on the determination of optimum values of parameters like pile-tip cone angle, contact stiffness and mesh size etc., which becomes imperative for the simulation of pile penetration process exhibiting a large deformation phenomenon. Post installation of the pile, the surrounding soil is subjected to a surficial surcharge to induce consolidation settlement of soil strata. In contrary to the in-place pile, the squeezing effect induced by the penetration process of a jacked pile leads to the dissipation of higher excess pore-water pressure and subsequent marked increase in the effective radial stress. Consequently, it further leads to a higher negative skin friction and greater drag load on the jacked pile.

Keywords: Pile installation; Negative skin friction; Neutral plane; Large deformation; Finite element analysis; Pile-tip cone angle; Contact stiffness.

1. Introduction

To support the demanding necessity of sustenance and resources in the coastal boundaries, more and more land reclamation projects being undertaken in the coastal areas and tidal flats all around the world in Canada, China, Malaysia, Scotland, Singapore and outer countries with extensive coastal boundaries (Hosseini and Rayhani, 2017; Lee et al., 2019; Wu et al., 2023). In this regard, several offshore and near-offshore infrastructures are becoming increasingly prevalent including the construction of offshore wind turbines, wind power plants, building infrastructures, high-speed railways, airports and harbour structures as well as artificially reclaimed coasts and islands (Igoe et al., 2013; Jeong et al., 2014; Liu et al., 2020; Shen et al., 2022; Sahu et al., 2024). Each of these infrastructure is primarily supported by pile foundations to transfer the load to the bearing stratum while bypassing the overlying soft consolidating medium. The near-offshore and offshore sites mostly comprise soft to medium marine clay deposits, soft coastal soils, self-consolidating dredger slurries and fills comprising clays and sands (Jeong et al., 2013; Liu et al., 2020; Wang et al., 2023; Ebrahimipour and Eslami, 2024). Unlike the pile installation procedure commonly adopted in the inland, driven piles are generally discarded as they lead to significant driving induced stress and increase in the pore-water pressure that subsequently leads to the reduction in the effective strength of the embedding medium (Hosseini and Rayhani, 2017). Hence, in such circumstance, installation procedures such as bored, rotary, augur or jacked piling remains to be a preferred option. The quasi-static jacking or push-in piling has ever gained popularity owing to the minimum vibration, displacement and disturbance emanated during their installation process (Igoe et al., 2013).

Negative skin friction (NSF) is often encountered for such piles installed in soft soils or consolidating fills. It is the downward drag that acts on the pile surface when the soil surrounding the pile undergoes comparatively larger settlement than the pile itself. The NSF-

induced settlement is common in the clayey soils due to various reasons such as consolidation of fill soil under its own weight (self-consolidation), application of surcharge load and fluctuation in the water table (Poulos and Davis, 1980). Early research in regard to NSF and its induced settlements majorly focused on field experiments. Fellenius (1972, 1984) and the references therein reveal the significant influence of negative skin friction in increasing the net axial load on pile with time. Further, NSF is also found to affect the group performance of the pile owing to additional settlement of the pile cap (Blanchet *et al*., 1980). In addition to the field experiments, laboratory-scale centrifuge studies are also available to understand the effect of pile loading conditions on the development of negative skin friction (Leung *et al*., 2004). Apart from the experimental investigations, literatures are also available on the numerical simulations exploring the evolution of negative skin friction on piles installed in soft soil (Comodromos *et al*., 2005; Lam *et al*., 2009; Liu *et al*., 2012), while addressing the influences of pile-group effect (Lee *et al*., 2001), interface friction coefficient (Jeong *et al*., 2004) and interface model behaviour (Cao *et al*., 2014). Although a number of literature are available on the influence of negative skin friction on the pile capacity, most of these numerical studies were conducted assuming the pile to be 'in-place' condition. In such type of modelling, the numerical approach considers the pile to be installed in-situ after replacing the corresponding volumetric domain of the soil. Hence, these studies do not take into account the pile jacking procedure that is often followed in the field.

Numerical simulation of the pile jacking process is very challenging due to the large deformation and excessive mesh distortion associated with it. Few literature (Carter *et al*., 1979; Randolph and Wroth, 1979; Randolph et al., 1979; Tolooiyan and Gavin, 2011) employed the cylindrical cavity expansion method to simulate the pile penetration process, which utilizes the horizontal expansion of a pre-defined cylindrical hole. This method is capable of assessing the shaft resistance; however, the accuracy of tip bearing resistance

remains debatable, especially for the jacking cases. In case of finite element based simulation, large deformation problems are usually addressed by 'Updated Lagrangian' and 'Coupled Eulerian-Lagrangian (CEL)' framework (Wang *et al*., 2015; Fan *et al*., 2021; Ghosh Dastider *et al*., 2022; Zhao *et al*., 2023). While simulating a large deformation problem like pile penetration, the updated Lagrangian approach often suffers from convergence issues (Mabsout and Tassoulas, 1994; Henke, 2010; Yi *et al*., 2012); however, there are evidences that its performance can be possibly improved by adjusting various parameters such as the contact properties, pile-tip cone angle and initial mesh configuration (Sheng *et al*., 2005, 2006, 2009, 2013), especially for a relatively smooth soil-pile interface. On the other hand, the arbitrary or coupled Eulerian-Lagrangian approaches does not exhibit such convergence issues (Walker and Yu, 2006; Liyanapathirana, 2009; Qiu *et al*., 2011; Pucker and Grabe, 2012; Tho *et al*., 2012; Sabetamal *et al*., 2014; Hamann *et al*., 2015; Fall *et al*., 2021). Capturing the evolution of pore-water pressure in a CEL framework can be achieved by using an analogy of heat transfer analysis as reported in Hamann *et al*. (2015). However, this approach can become very complex, thereby requiring special attention while determining the same through available FEM packages. Further, in recent times, the large deformation problems involving dissipation of excess pore-water pressure as encountered during the pile or cone penetrations has also been addressed by the use of coupled PFEM i.e. particle finite element method (Monforte *et al*., 2018; Yuan *et al*., 2019) and coupled MPM i.e. material point methods (Ceccato *et al*., 2016; Ceccato and Simonini, 2017). Although many of the previous works successfully simulated the large deformation process associated with the pile penetration problems within a numerical framework, the effect of the pile installation method on the manifestation of negative skin friction is yet to be addressed.

The primary focus of the present study is to explore numerically the evolution of negative skin friction on a pile inserted in multi-layered soft soil substrata by employing two

different installation schemes. The first installation scheme represents a jacked pile, where the pile penetration process is simulated by inserting the pile into the soil domain at a constant rate. The second installation scheme, which is more commonly adopted from a numerical perspective due to its convenience and ease, considers the pile to be 'wish in-place', where the pile is considered installed by replacing an identical volumetric region as that of the pile from the corresponding soil material. The large deformation based geometrically non-linear problem of pile penetration process has been simulated in FEM by applying updated Lagrangian approach (as per Belytschko *et al.*, 2001) with suitable control over various simulation parameters and employing a relatively smooth soil-pile interface. An associative Modified Cam Clay model that can efficiently capture the non-linear elastoplastic constitutive response of soil has been used in this study. Contact non-linearity has been considered at the soil-pile interface, where the contact is numerically enforced through the penalty method (Wriggers, 2006). Determination of optimum values of parameters such as cone angle, contact parameter and mesh size have been carried out, as they are imperative for an effective large-deformation based finite element simulation of pile penetration. The simulation results are validated against a case study reported by Indraratna *et al.* (1992) where bitumen coated piles were penetrated into soft Bangkok clay. The pore-water pressure (PWP) data obtained from the field test at different depths have been used to validate the performance of the numerical model. Further, surficial surcharge (fill load) in the periphery of the pile has been applied to induce negative skin friction by permitting consolidation of the soft soil surrounding the pile. Subsequently, the two different pile installation schemes are simulated numerically and the development of negative skin friction in their post-surcharge response are critically analysed in terms of the development of shear stress, drag load, effective radial stress, and the position of neutral plane.

2. Simulation of pile jacking process

In the reference literature that has been used for the validation study, Indraratna *et al*. (1992) reported penetration of a bitumen coated pile through soft Bangkok clay at a very slow penetration rate of 1 m/min. In the present study, the same penetration rate (1 m/min) is employed during the simulation of pile jacking process within an updated Lagrangian framework in Abaqus version 6.14. As a result of the slow penetration rate in the field, a quasi-static penetration has been carried out neglecting inertial forces. A similar approach for modelling pile jacking can also be found in literature (Wang *et al*., 2015; Fan *et al*., 2018, 2021). A detailed discussion on model geometry, boundary conditions, material properties, and other simulation parameters like mesh discretisation, contact stiffness, adopted pile-tip cone angle and influence of soil domain have been presented in this section along with a validation against a field study.

2.1 Model geometry

An axisymmetric 2D model has been used to simulate the penetration of a cylindrical pile through the soft soil. The pile considered in the study is 20 m long and has a diameter of 0.4 m. In this regard, a soil domain having 40 m depth (twice the length of the pile) and 30 m radial distance has been selected for the simulation (Fig. 1). Due to the accumulation of excessive stress at the pile base, the penetration of a flat-ended pile into the soil is quite difficult with the current contact theories. Given the various types of pile tip used in practice, a study has been performed on the possible variation of the pile-tip cone angle, and an optimal cone angle of 60º has been selected in the simulation. The effect of cone angle on the penetration process has been discussed in detail in a subsequent section.

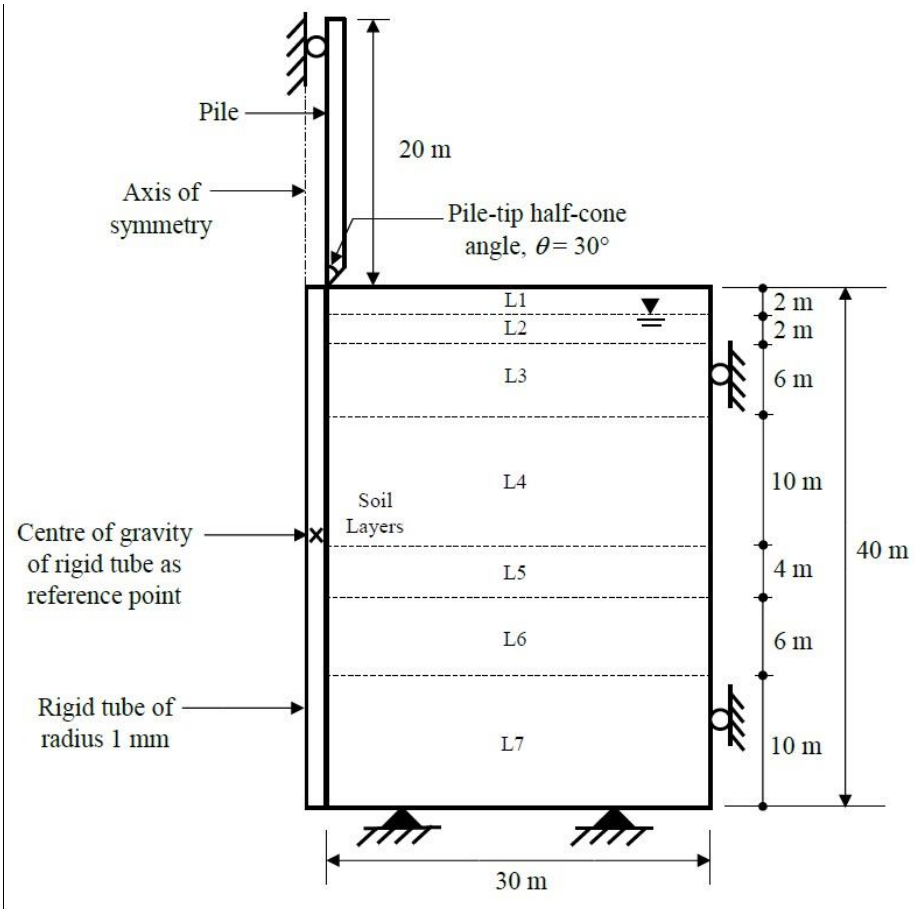

Fig. 1: Schematic representation of the axisymmetric model used for the simulation of pile jacking process (Figure dimensions are not to scale).

In an axisymmetric formulation, the boundary at the axis of symmetry usually remains constrained from displacing in the horizontal direction during the FE simulation. However, such constraint cannot be imposed for the pile penetration simulation due to radial distortion of the soil adjacent to the pile. An alternate solution for such scenario is to provide a narrow rigid solid tube at the axis of symmetry and enforcing a total fixity condition at its centre of gravity (Yi *et al*., 2012; Ekanayake *et al*., 2013). Following the same, for this study, a rigid solid tube of 1 mm radius has been provided at the axis of symmetry in order to allow the radial movement of the soil during the penetration process. Interaction between the tube-soil and tube-pile interface has been kept frictionless for both types of pile installation cases. Figure 1

shows the placement of the rigid tube and pile in the axisymmetric model for the pile jacking case.

2.2 Boundary conditions

The displacement boundary conditions have been applied to the pile head, at the centre of rigid tube, and to the bottom and right lateral boundaries of the soil domain (Fig. 1). The pile penetration procedure has been simulated through the applied displacement boundary condition at the pile head and subsequent adjustment of the time step such that the penetration velocity of the pile remains constant at 1 m/min throughout the jacking process. The motion of rigid tube has been restricted in both the lateral and vertical directions by applying total fixities at a reference point conforming to its centre of gravity. The far lateral boundary of the soil domain has been restricted from radial movement by applying horizontal constraint, while total fixity is applied at the bottom boundary, as shown in Fig. 1. Following the actual case study (Indraratna *et al*., 1992), water table has been assumed located at 2 m depth below the ground surface, and the soil above the water table has been assumed fully saturated due to capillary rise. Hence, for modelling the initial geostatic stresses, a zero PWP boundary condition has been applied at the depth of 2 m (ensuring a complete drainage boundary). Initial stresses within the soil domain, prior to the jacking, have been generated by applying a gravity loading condition; whereas, during the jacking process, a body force has been enforced on the pile by specifying its unit weight.

2.3 Material properties

An associative modified Cam clay (MCC) model has been selected to capture the non-linear elastoplastic constitutive response of the soil. The parameters of modified cam-clay

model for various soil layers have been obtained from the case study by Indraratna *et al*. (1992). The initial void ratio has been estimated from the reported critical state parameters and field undrained shear strength data. The undrained shear strength (S_u) is obtained from the following relation derived from the critical state concepts:

$$S_u = \frac{q_f}{2} = \frac{M}{2}\exp\left(\frac{e_\Gamma - e_{init}}{\lambda}\right), \quad (1)$$

where q_f is the deviatoric stress at failure, e_Γ is the void ratio on the critical state line at reference pressure, e_{init} is the initial void ratio, M and λ are slopes of the critical state line in stress (p-q) and volume (e-ln p) space, respectively. The pile and soil material properties used in this study for the finite element simulation have been listed in Table 1 and Table 2, respectively.

Table 1: Material properties of the pile used in the FE model.

Young Modulus E **(kN/m^2)**	**Diameter** D **(m)**	**Poisson's ratio** μ	**Unit weight** γ **(kN/m^3)**
30×10^6	0.4	0.33	15

200 Table 2: Material properties of the soils used in the FE model.

Layer No.	Layer	γ_d (kN/m^3)	μ	E (kPa)	M	k	λ	e_{int}	p_c (kPa)	K_o	k_i (m/day) ($\times 10^{-4}$)	OCR	S_u (kPa)
L1	Weathered clay (0-2)	11.65	0.33	-	1.05	0.05	0.18	1.32	22.2	0.716	6.76	3	29.4
L2	Weathered clay (2-4)	11.65	0.33	-	1.05	0.05	0.18	1.32	55.31	0.716	6.76	3	29.4
L3	Soft clay (4-10)	7.22	0.33	-	0.97	0.08	0.51	2.67	35.58	0.62	0.55	1.2	12.1
L4	Soft clay (10-20)	10.23	0.33	-	0.98	0.06	0.32	1.59	59.41	0.661	0.26	1.2	26.6
L5	Medium stiff clay (20-24)	13.45	0.33	-	0.9	0.03	0.12	0.97	103.23	0.666	0.37	1.4	42.1
L6	Stiff clay + sand (24-30)	14.48	0.33	-	0.9	0.03	0.12	0.83	140.9	0.685	0.37	1.5	252.6
L7	Stiff clay + sand (30-40)	14.02	0.33	27440	-	-	-	0.89	189.62	0.685	0.37	-	-

201 *The symbols referred in the table indicates the following: γ_d = dry unit weight of soil, μ = Poisson's ratio, E = Young's modulus, M = slope of
202 the critical state line in stress (p-q) space, k =slope of the unloading line in volume (e-ln p) space, λ = slope of the critical state line in volume (e-
203 ln p) space, e_{init} = initial void ratio, p_c = pre-consolidation pressure, K_o = lateral earth pressure coefficient at rest, k_i = coefficient of permeability,
204 OCR = over-consolidation ratio, S_u = undrained shear strength.

2.4 Mesh convergence study

As stated earlier, numerical simulation of pile penetration process involves severe distortion of elements. Such distortions become more prominent during simulations with finer mesh and produce negative determinant of the Jacobian matrix (Bathe, 1996; Sheng *et al*., 2009), which ultimately results in non-physical negative element stiffness. The selection of a coarser mesh can avoid the excessive element distortion, but it provides crude results due to lesser discretization of the domain. Hence, three different single-biased meshes (comprising finer discretisation near the pile-soil interface and coarser discretisation towards the far lateral boundary) have been considered for the convergence study and the details of which is given in Table 3.

Table 3: Mesh sizes selected for convergence study.

Sl. No.	Mesh	Mesh size (m)			
		Along radial direction from axis of symmetry		Along the depth from ground surface	
		0 to 10 m	10 to 30 m	0 to 30 m	30 to 40 m
1	Medium	0.5 to 1	1 to 2	0.5	0.5 to 1
2	Fine	0.2 to 1	1 to 2	0.2	0.2 to 1
3	Very fine	0.1 to 1	1 to 2	0.1	0.1 to1

Seeding has been done in such a way that the elements near the pile have an aspect ratio of 1. As the region farther from the pile is expected to have lesser influence of jacking process, lower mesh density has been assigned in that region. Owing to the higher rigidity of the pile compared to the surrounding soil, the pile is expected to undergo less distortion and hence,

larger element size has been assigned for the pile. The pile has been discretized with CAX4 element (4-noded bilinear axisymmetric quadrilateral element), while CAX4P element (4-noded axisymmetric quadrilateral element with bilinear displacement and bilinear pore pressure) has been chosen for discretizing the soil domain. An attempt has been made to generate a structured mesh that will predominantly comprise of rectangular elements. The convergence study has been carried out by jacking the pile up to a depth of 8 m into the soil, with a penetration rate of 1 m/min. It is to be noted that a penetration depth of only 8 m has been chosen for performing the mesh convergence study in order to economize the computational time. For the remaining part of the study, a full depth penetration of the pile (i.e. 20 m) has been considered.

Figure 2 shows the load-displacement curves, estimated at the pile head, for the three types of mesh densities used in this study. Although the mean value of load-displacement curves looks similar, smoother curves have been obtained by adopting finer meshes, while the coarser meshes exhibited significant oscillations in the results. Such oscillations in the quasi-static pile penetration are a feature commonly observed in penetration problems (Simo and Meschke, 1993; Sheng *et al*., 2013; Kouretzis *et al*., 2014; Fan *et al*., 2018, 2021) and is not attributed to be an indicator of numerical instability. The oscillations in the contact forces are primarily attributed to the sudden change in the normal direction along the penetrating body, i.e. at corners or vertices (Sheng *et al*., 2006, 2009). With the change in the normal direction, a sudden reduction in the vertical reaction force occurs when a soil node traverses around the sharp corner, the effect of which is magnified for the low-density meshes. The type of scheme adopted for the contact surface discretization can further impact such oscillatory nature (Sheng *et al*., 2009; Aubram *et al*., 2015; Wang *et al*., 2015). In general, a finer mesh discretization reduces these oscillations (Sheng *et al*., 2009) and the same has been adopted in this study. Based on the results of mesh convergence study, finally, a ‘very fine’ single-biased mesh has

247 been selected (Fig. 3) for further simulations, such that the elements of 0.1 m size would be
248 present just beneath the pile tip. The selected size is exactly half of the radius of the pile and
249 satisfies the proposition by Sheng *et al*. (2005), which states that the soil elements just beneath
250 the pile should have a size ranging between 0.5-1.0 times the pile element size in order to obtain
251 appreciable results without any convergence issues. The combination of mesh discretization
252 and contact parameters are very important to ensure the optimal performance of the numerical
253 simulation. The details of the contact modelling employed for the soil-pile interface has been
254 discussed in the following section.

255

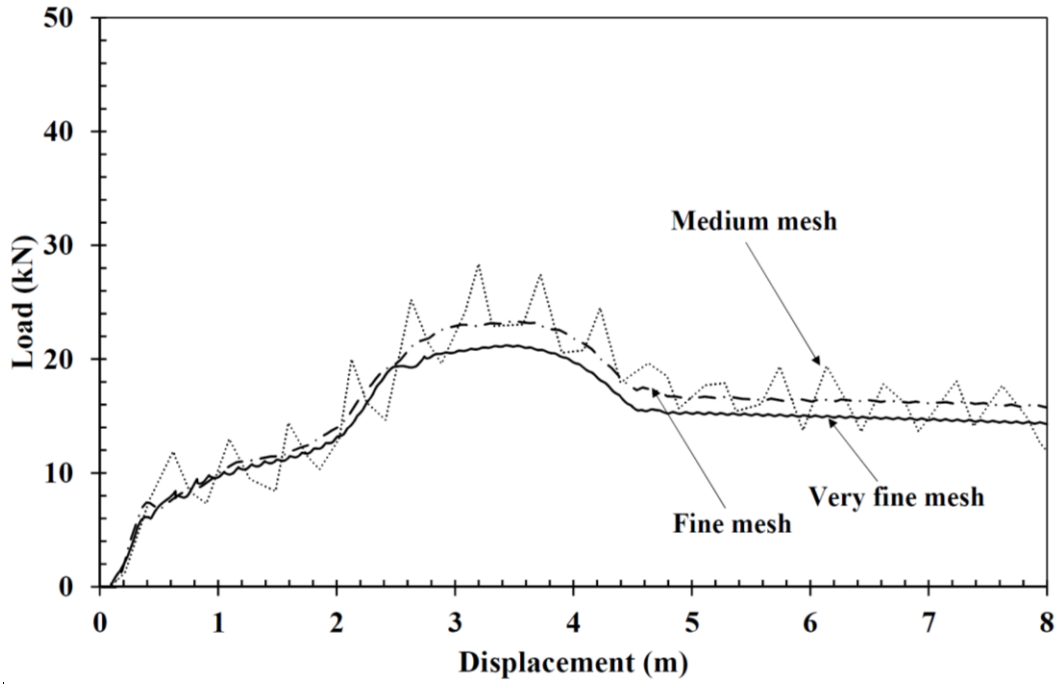

256

257 Fig. 2: Load-displacement curve for different mesh densities.

258

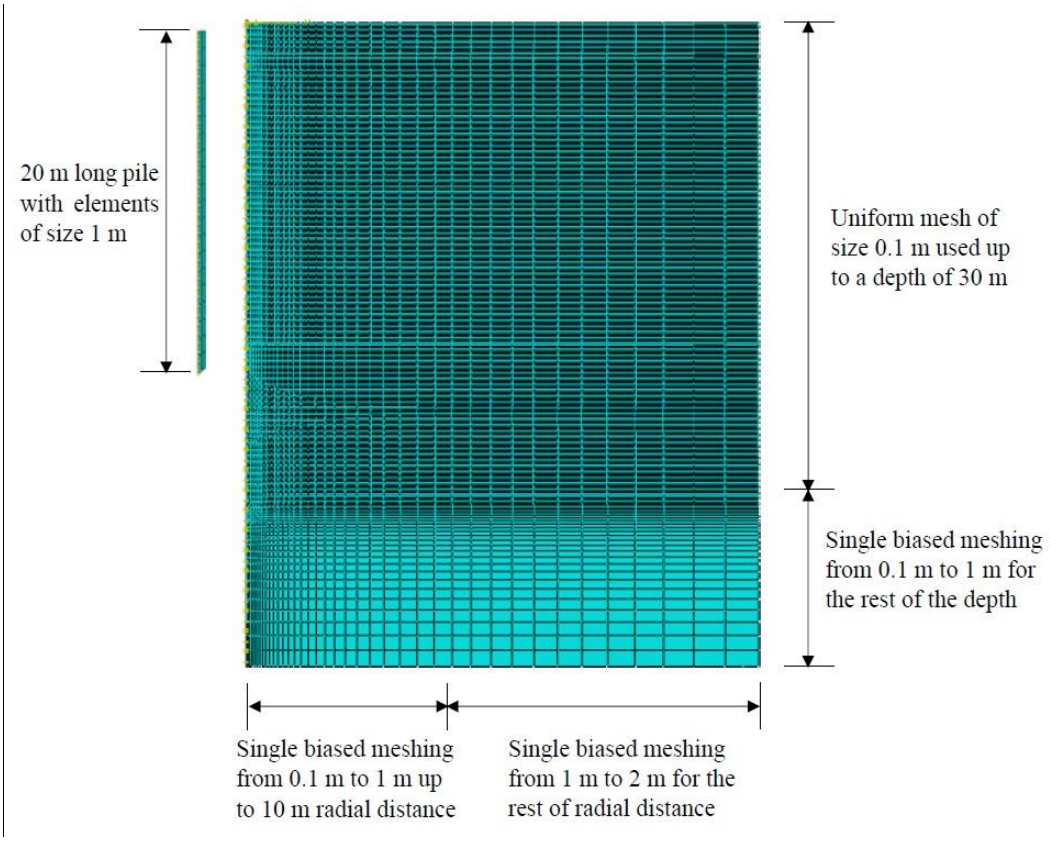

Fig. 3: Discretization and meshing adopted for the soil domain and pile for the present study (Figure dimensions are not to scale).

2.5 Selection of contact stiffness parameter

Lagrangian multiplier and penalty method are widely used to enforce the normal contact constraints in FEM (Wriggers, 2006); therefore, these two methods have been tested for their suitability in this simulation. Lagrangian multiplier method has been used in the preliminary trial simulations, which exhibited convergence issues and required higher computational time. Hence, the simulations are further carried out in this study applying the penalty approach, which allows small penetration at the soil-pile interface. It is important to note that the selection of a lower penalty stiffness reduces the convergence issues; however, it can increase the penetration at soil-pile interface leading to unrealistic solution. Hence, the selection of a proper penalty stiffness is an important decision in order to acquire reliable results. The value of penalty stiffness has been obtained here by an iterative approach. Initially,

a very small value of penalty stiffness, $\varepsilon = 10^4$ kPa/m has been selected for the iteration with a smooth soil-pile interface. The chosen smooth soil-pile interface condition conforms to the very low frictional resistance offered by the bitumen coated pile used in the field study reported by Indraratna *et al*. (1992). A surface-to-surface contact has been provided at the soil-pile interface. The pile having more rigidity than the soil has been assigned as the master surface; whereas, the soil is considered to act as slave surface. Subsequently, the stiffness value has been increased gradually and the load-displacement curves are plotted to monitor the response of the penetration process.

The general trend observed in the load-displacement plot can be attributed to the variation in soil stratification in terms of their density, stiffness and undrained shear strength (Table 2). The variations of the layer properties result in the sudden changes in the reaction force as the pile traverses into the successive soil layers, and a detailed discussion on the same has been presented in the next section. It has been further noticed that with increase in the penalty stiffness, the magnitude of reaction force gradually increases and attains higher values. However, the load-displacement curves begin to portray significant spuriousness and oscillations, especially for $\varepsilon > 2\times10^4$ kPa/m, which is attributed to the stiff contact constraint at the nodes (Fischer *et al*., 2007). This is further illustrated through the load-displacement curve presented in Fig. 4a for different penalty stiffness. It can be noticed that the load-displacement response for penalty stiffness $\varepsilon = 10^4$ kPa/m is quite smooth; however, at any displacement level, it exhibits considerably lower magnitude of load than those obtained from the higher stiffness parameters. On the other hand, a higher stiffness parameter gives higher load-displacement response but laden with oscillations. Figure 4(b and c) show the post-penetration distorted mesh pattern at 20 m soil depth, as obtained from the penalty stiffness $\varepsilon = 10^4$ kPa/m and 2×10^4 kPa/m, respectively. It can be observed that penalty stiffness has significant effect on the mesh distortion and higher penetration has been recorded at the soil-

pile interface for ε =10^4 kPa/m when compared to the case with stiffness ε =2×10^4 kPa/m. Based on the above observations, a penalty stiffness of ε =10^4 kPa/m has been selected for 0-10 m pile depth and ε =2×10^4 kPa/m for 10-20 m pile depth. Considering the fact that the penalty stiffness depends on the stiffness of the bodies in contact and owing to the pressure-dependent nature of soil resulting in increased stiffness with depth, a higher value of contact stiffness is judiciously assigned to the lower part of the pile-soil interface as compared to the upper part. Besides making a judgement of the penalty parameter from the spuriousness and oscillations, it is worth mentioning that the contact stiffness can also be determined with the aid of iterative adjustments of the penalty stiffness while ensuring the inter-penetration of the contact surfaces remains within a tolerable limit (Wriggers, 2006).

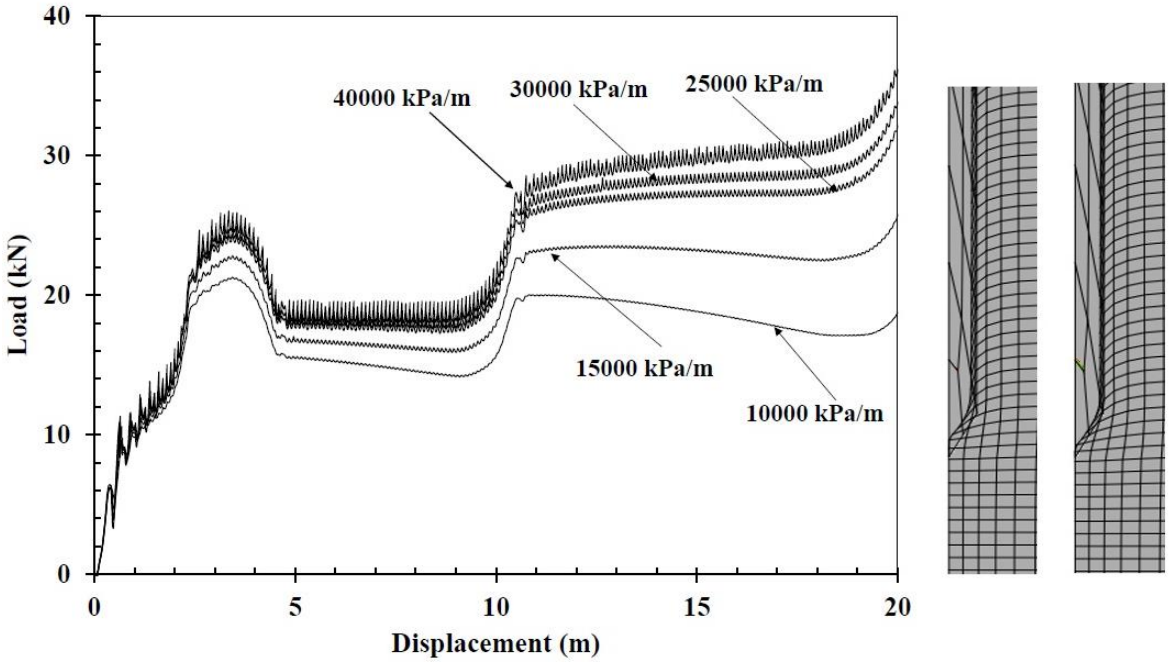

(a) (b) (c)

Fig. 4: (a) Load-displacement curve for different penalty stiffness, and post penetration distorted mesh pattern as obtained from two penalty stiffness (b) ε = 10^4 kPa/m and (c) ε = 2×10^4 kPa/m, respectively.

2.6 Influence of pile-tip cone angle

Selection of the proper pile-tip cone angle is essential for simulating any pile penetration related field study. Preliminary trials highlighted that the penetration of a flat-tip pile causes excessive distortion of mesh and creates convergence issues. The influence of cone angle on the pile penetration response has been explored by performing simulations with a pile of 20 m length and 0.4 m diameter, and having pile-tip half-cone angles (θ, see Figure 1) ranging from 15º to 45º. In this regard, the load-displacement and excess PWP dissipation responses are assessed for determining the optimum cone angle suitable for simulation of the pile penetration process.

Figure 5(a) shows the development of reaction force during the penetration process for three different pile-tip half-cone angles, i.e. 15º, 30º and 45º. A similar trend can be noticed in the load-displacement response obtained for all the adopted half-cone angles. It is worth mentioning that due to the assumption of smooth soil-pile interface, the pile jacking simulation neglects the contribution of shaft resistance towards mobilization of the load-displacement response. As a result, the load-displacement is solely governed by the pile tip resistance which is significantly guided by the stratification characteristics of the substrata, namely the density, stiffness and undrained shear strength variation along the depth. It can be observed from Table 2 that the average undrained shear strength of the soft clay layer located within the depth 4-10 m (~ 12.1 kPa) is lower than that of the weathered clay layer spanning within 0-4 m (~ 29.4 kPa) from the ground surface. As the pile penetrates through the weathered clay layer, the resistance increases, which starts to decrease from 4 m depth onward as the pile tip reaches the soft clay layer. With the continued penetration of the pile through the soft clay layer, the load-displacement response remains nearly constant until the depth of 10 m, where the pile tip encounters the next soft clay layer having relatively higher average undrained shear strength (~ 26.6 kPa). Consequently, an increase in the resistance can be noticed, followed by a nearly

342 constant load-displacement response as the penetration continues through this layer.
343 Furthermore, as the pile tip reaches the medium stiff clay layer at a depth of 18 m, a successive
344 increase in the resistance is observed due to the markedly higher undrained shear strength of
345 the layer.

346 Further, from Fig. 5(a), it can be observed that with the increase of half-cone angle, the
347 magnitude of load at a given displacement are understandably higher. A blunt pile tip is
348 expected to disturb a larger soil mass during the penetration process resulting in a larger
349 influence zone in comparison to the piles with sharper tips. Figure 6(a-f) depicts the radial
350 displacement (U1) and axial displacement (U2) contours near the pile tip for various half-cone
351 angles. It can be noticed that the influence area corresponding to the pile with 45º half-cone
352 angle is maximum when compared to the remaining cases of piles with relatively sharper tips.
353 Since the pile with 45º half-cone angle displaces larger soil mass, higher axial load is required
354 for its penetration to a given depth. This can be further explored from the contours of the
355 mobilized shear stress (S12) around the pile tip for different cone angle (Fig. 6g-i). It can be
356 observed that the magnitude of the mobilized shear stress for the pile with 15º half-cone angle
357 is comparatively low while the pile with 45º half-cone angle exhibits the largest influence zone.
358 Apart from the magnitude, higher oscillations are also observed in case of a 45º half-cone angle,
359 which gradually disappeared with further reduction in the pile-tip half-cone angles (Fig. 5a).

360 Figure 5b shows the dissipation of PWP near the tip of the pile at a depth of 20 m for a
361 post-pile installation period of 1000 days. It can be noticed that after the end of the penetration
362 process, pile tip with 45º half-cone angle has maximum excess PWP and the same gradually
363 reduces with the reduction in the half-cone angle. However, after 100 days, the excess PWP
364 dissipation profiles become very similar for all the chosen half-cone angles. A half-cone angle
365 of 30º has been selected for the present study that induces less oscillation in the load-
366 displacement response and yet have intermediate variation in the excess PWP magnitude after

the completion of penetration step. For both the jacked and in-place cases, a 30º half-cone angle has been used throughout the rest of the simulations.

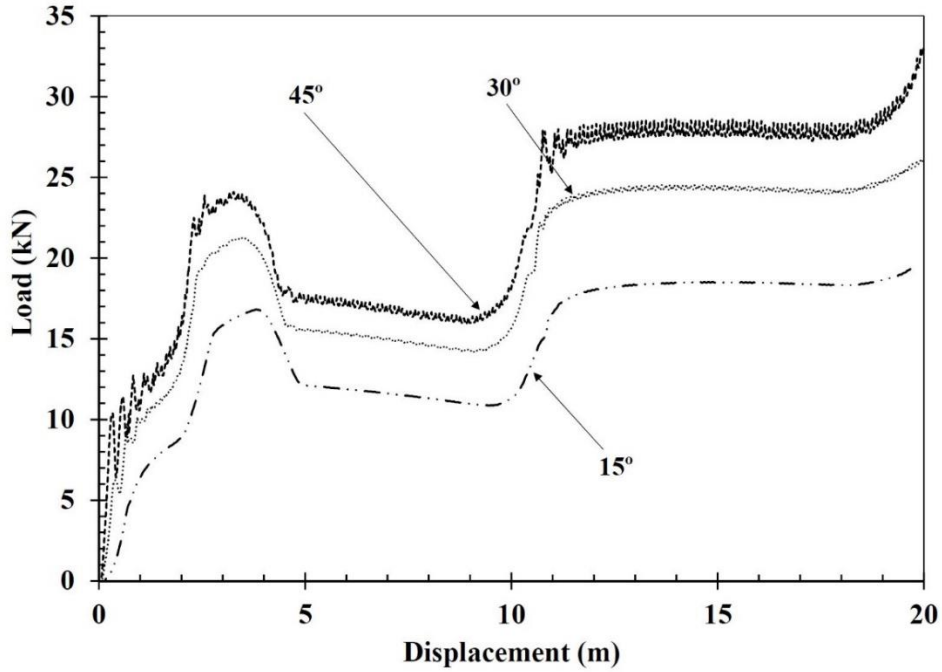

(a)

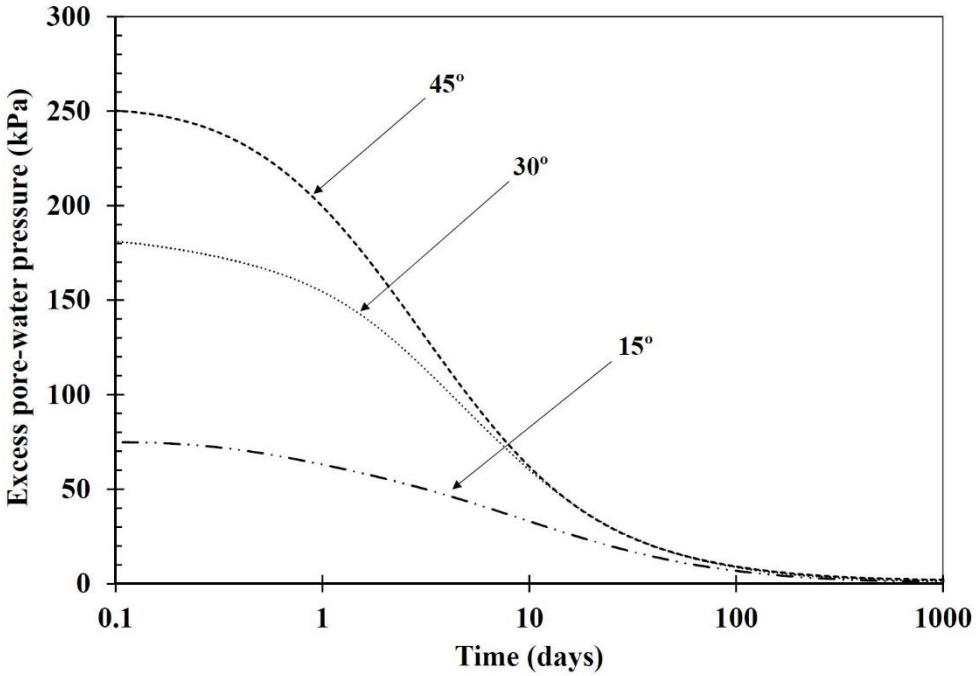

(b)

Fig. 5: (a) Load-displacement response during the penetration process, and (b) excess pore-water pressure dissipation near the pile tip during the post-penetration period for pile-tip half-cone angle $\theta = 15º$, 30º and 45º.

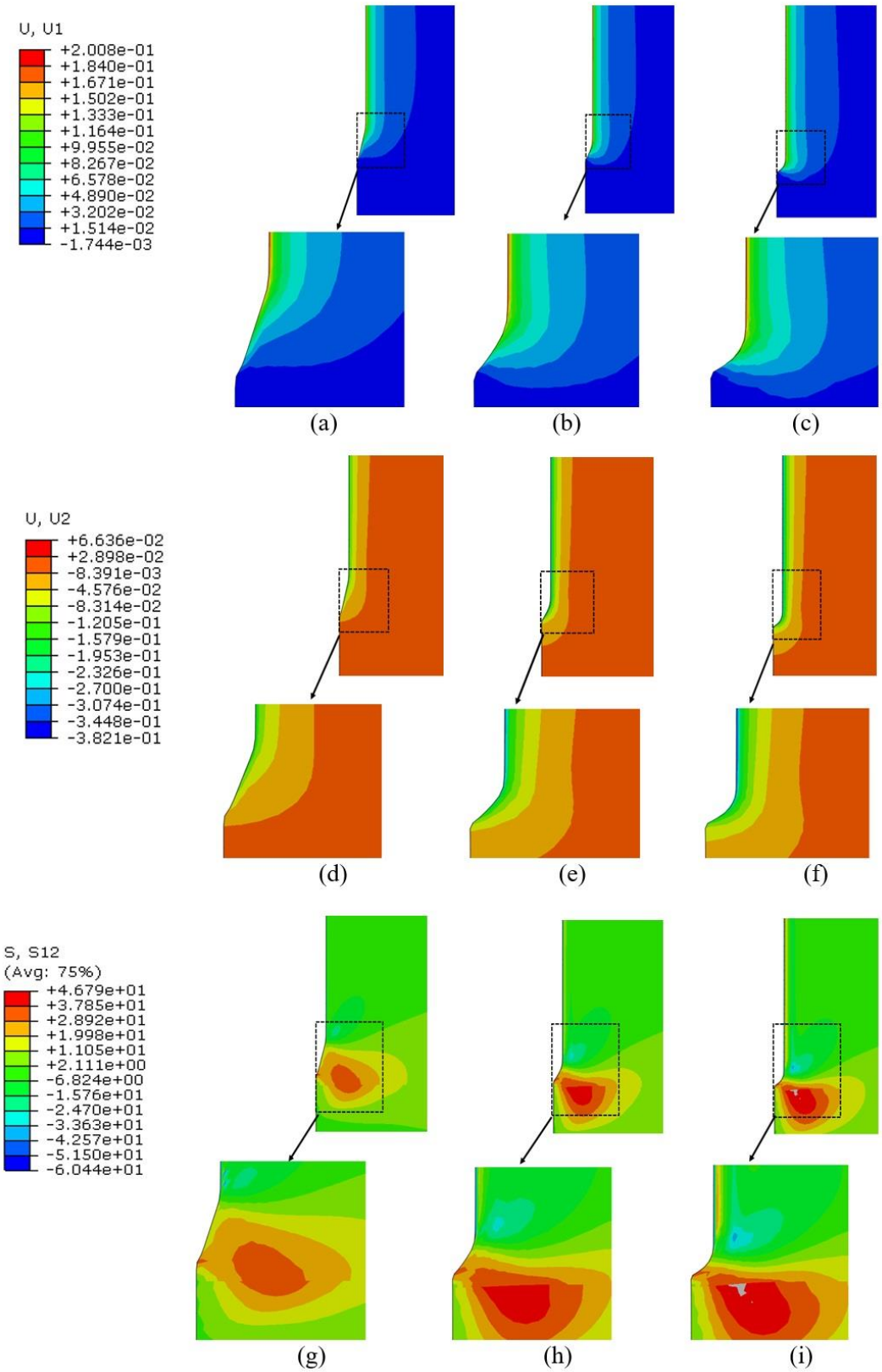

Fig. 6: Contours of (a-c) radial displacement U1, in m, (d-f) axial displacement U2, in m, and (g-i) shear stress S12, in kPa, near the tip for θ = 15º, 30º and 45º pile-tip half-cone angles, respectively.

382 **2.7 Influence of selected soil domain**

383 In this section, suitability of the selected soil domain has been examined through the
384 increment in effective radial stress and excess PWP distribution. For this purpose, after the pile
385 has penetrated to its full depth of 20 m, the increment in effective radial stress and excess PWP
386 data are obtained and are plotted along the radial path passing through a depth of 20 m from
387 the ground surface, as shown in Fig. 7(a-b). It has been noticed that the penetration process
388 does not impart any significant influence on the effective radial stress beyond a radial distance
389 of 10 m from the axis of symmetry (i.e. 25D) (Fig. 7a). Similarly, the excess PWP plot shows
390 negligible change beyond a 3 m radial distance from the pile (i.e. 7.5D) (Fig. 7b). A rapid
391 decrease in the excess PWP is observed along the radial distance, which is consistent with the
392 observations reported by Hwang *et al*. (2001). Figure 7 (c-d) shows the contour plot of total
393 PWP (or, POR) before and after the penetration process, respectively, and it can be observed
394 that the influence of penetration process becomes negligible beyond a depth of 30 m (i.e. 25D
395 from the pile tip) Further, the effective radial stress (S11) contour, before and after the pile
396 penetration process, has been plotted in Fig. 7(e-f). It clearly indicates that the effect of pile
397 penetration is localized only in the region adjacent to the pile and beyond a depth of 30 m, the
398 pile penetration process does not impose any recognizable influence on the generated radial
399 stresses. Hence, it can be concluded that the selected soil domain, i.e. 30 m radial distance (i.e.
400 75D) and 40 m vertical depth (i.e. 100D), is apt and would pose no boundary influence on the
401 simulation of the pile penetration process or the associated post penetration analysis.

402

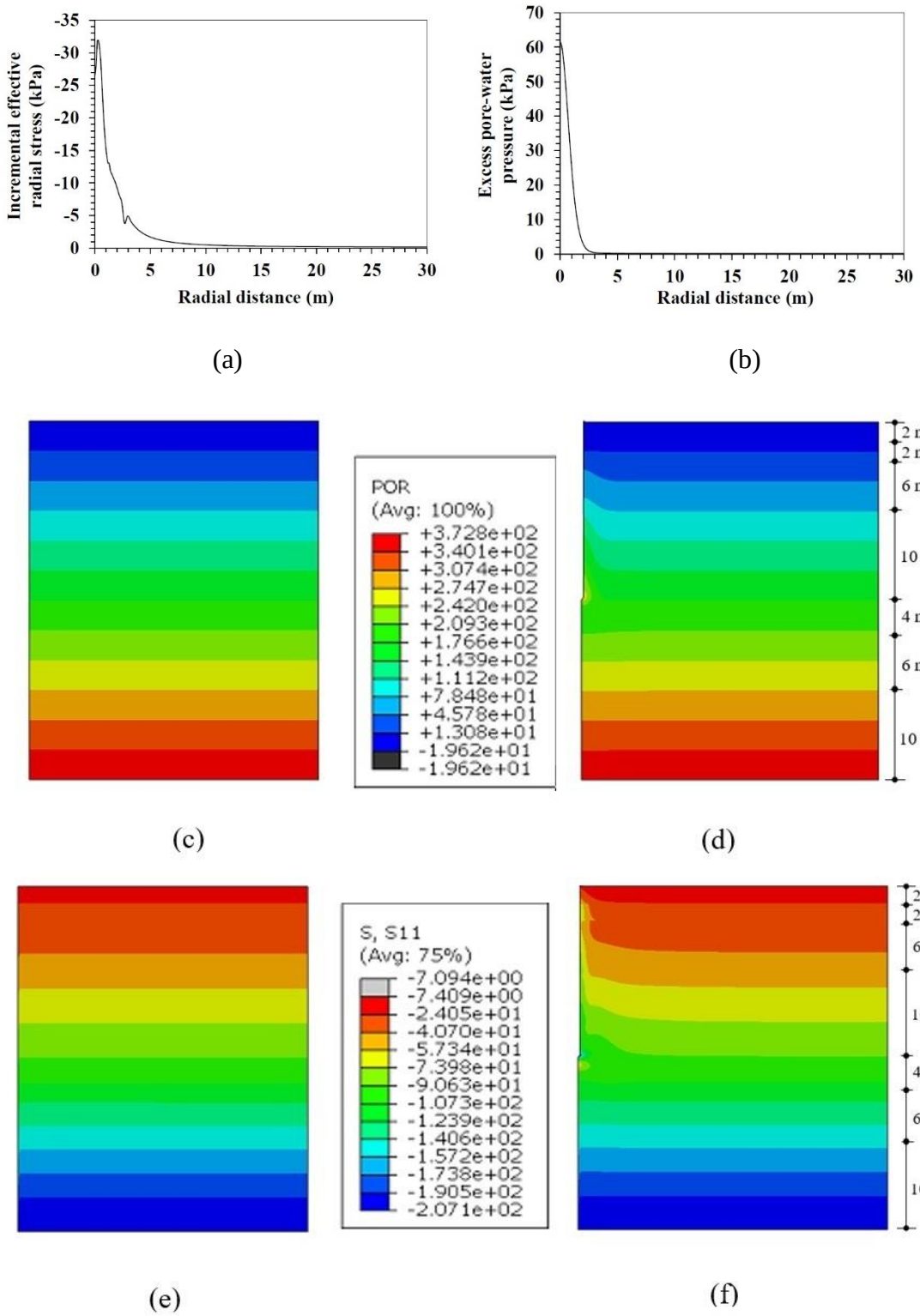

Fig. 7: (a, b) Increase in effective radial stress and excess pore-water pressure variation along a radial path at a depth of 20 m just after the pile penetration, (c, d) total pore-water pressure contour (POR, in kPa) before and after the pile penetration process, (e, f) effective radial stress contour (S11, in kPa) before and after the pile penetration process, respectively.

411 **2.8 Validation**

412 The simulation-based penetration responses have been compared and validated against
413 those reported by Indraratna *et al*. (1992), where a case study has been reported for a bitumen-
414 coated pile that was penetrated through soft soil up to 20 m depth and excess PWP dissipation
415 data were recorded by the piezometers. The bitumen-coated pile, in general, is expected to have
416 a significantly lower interface friction and hence, the validation study has been carried out
417 assuming a smooth soil-pile interface. This also gets substantiated by the results reported by
418 Indraratna *et al*. (1992) where the negative skin friction along the bitumen-coated pile was, on
419 an average, 50% lower than that developed in the uncoated pile (possessing higher interface
420 friction). This translated to the maximum axial load in the coated pile being 2.5 times lesser
421 than that of the uncoated one. In the referred field study, the pile penetration was performed at
422 a constant rate of 1 m/min, and the same sequence followed in the actual case study have been
423 replicated in the simulation. These include step-wise penetration of the pile up to certain
424 intermediate depths, i.e. first 8 m and then at penetration increment of 4 m, such that each of
425 these penetration steps has been followed by a consolidation phase for a duration of 8 days.
426 This complete process takes 2766000 s (approximately 32 days).

427 After the simulation of the above steps, excess PWP dissipation data, recorded for eight
428 successive days at 8 m and 20 m penetration depths, have been plotted against elapsed time
429 and compared to the corresponding field measurements during the post-penetration durations,
430 as shown in Fig 8(a) and (b), respectively. As the position of pile tip never coincides with the
431 soil nodes, an average value of excess PWP, calculated from the nodes just above and below
432 the pile tip, has been reported here. The simulation results are found to compare well against
433 the field data reported by Indraratna *et al*. (1992). The accurate measurement of excess PWP
434 data in field is an extremely difficult process which will also have its implications on the slight
435 variations noticed between the simulated results and the reported field data. It is important to

note here that the initial pore-water pressure dissipation characteristics is largely governed by the amount of excess pore-water pressure generated during the penetration phase. In this regard, Indraratna *et al*. (1992) has clearly reported that a significant scatter in the pore-water pressure time-history had been noticed for multiple piezometer locations. Further, it has also been mentioned that the presence of undissipated pore-water pressure due to the pile penetration process has induced some complications in the monitoring of the actual pore-water pressures in the consolidating clay layer, which might attribute to the sudden decrease in the recorded initial pore-water pressure dissipation profile. Given all the possible sources of uncertainty in the field measurements thereby leading to some marginal deviations, it can be yet noticed that the simulation is successful in aptly capturing (i) the magnitude of excess pore pressure generated just after pile penetration and (ii) the general trend in the long-term dissipation of excess pore-water pressure.

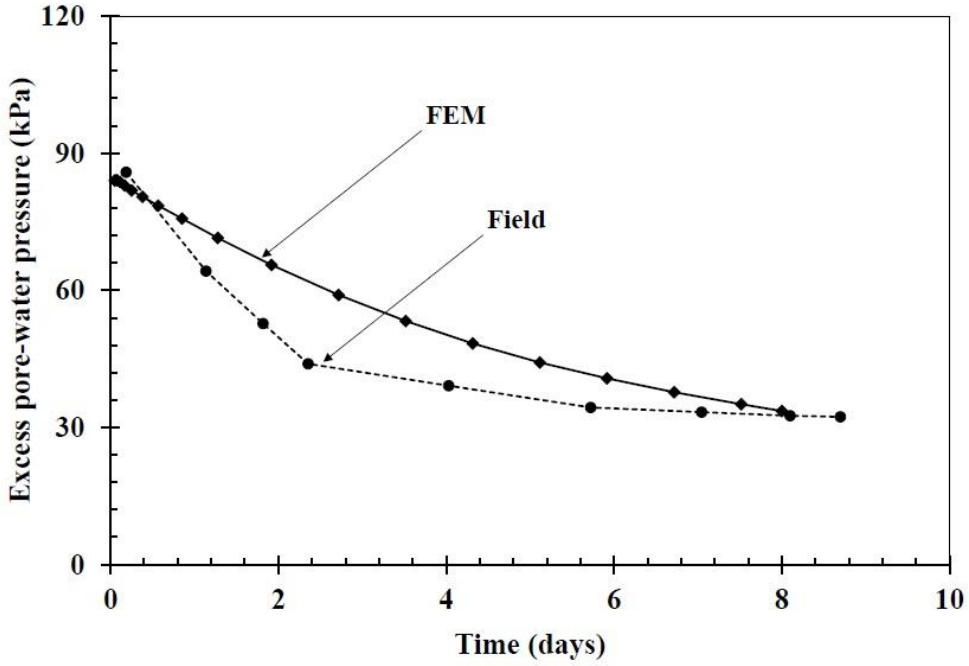

(a)

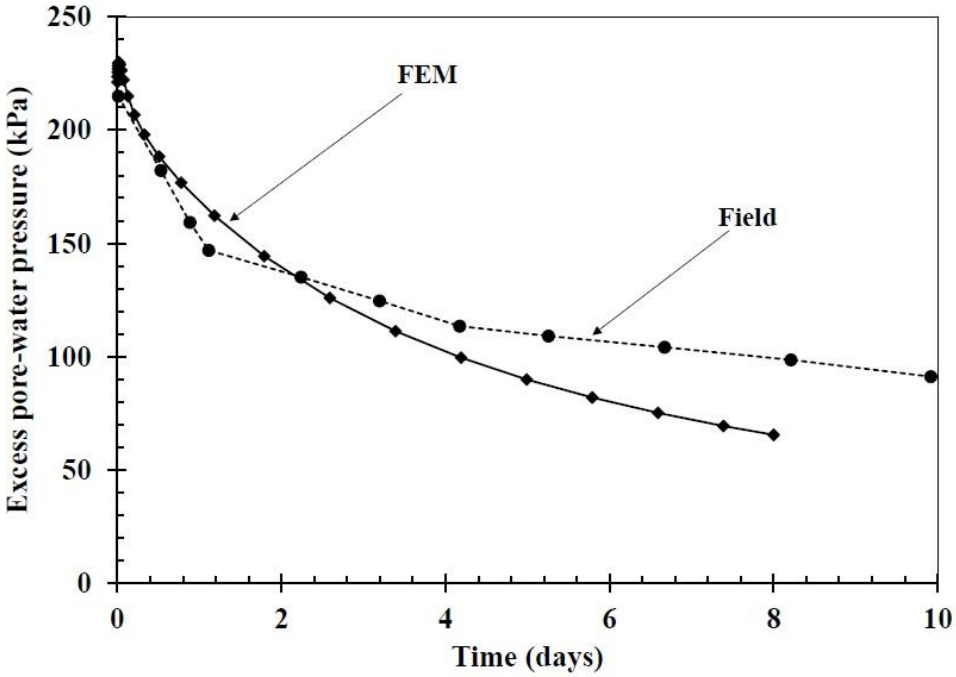

(b)

Fig. 8: Comparison of the excess pore-water pressure dissipation between field records and FEM simulations at depths (a) 8 m and (b) 20 m, respectively, during the post-penetration consolidation period.

3. Post jacking simulation

After the completion of pile jacking, a surcharge load has been applied over the soil surface for the successive generation of negative skin friction. In order to explore the effect of jacked and in-place methods on the development of negative skin friction, this has been further followed by a consolidation step in the simulation process. A 10 m radius cylindrical surcharge loading with surface stress intensity of 34 kPa has been applied only on the surrounding soil, without applying the same on the pile head.

Interfacial friction is essential in order to generate the negative skin friction on the pile. The Coulomb friction model has been employed here to simulate the soil-pile interface. As the simulations are carried out for the bitumen coated pile, a low value of the frictional coefficient,

μ_f = 0.1, has been employed for the soil-pile interface. Even after applying all the earlier referred pre-processing steps (i.e., selection of half-cone angle, contact stiffness parameter and optimal mesh discretization) and interface properties, simulation of pile penetration process can be extremely difficult due to severe element distortion at the pile-soil interface. In order to resolve this issue, an automatic stabilization scheme has been used with a constant damping factor. This damping factor has been determined in such a way that the dissipated energy fraction remains equal to a nominal value of 0.0002 (Abaqus User's Manual, 2018).

The geometry, material properties and the other model parameters are kept similar for both jacked and in-place cases as mentioned earlier. After the completion of penetration process, a surcharge load of 34 kPa has been applied over the surrounding soil in a step of 86400 s (1 day). Further, the soil has been allowed to consolidate until the excess PWP in the soil get substantially dissipated, and this process has been carried out for a time period of 17000 days (1.47×10^9 s). It is to be noted that the only difference for the 'in-place' case is that the pile has been placed after replacing the soil mass without allowing any penetration and hence, no displacement boundary condition is required to be imposed on the pile head.

4. Post-surcharge loading response of jacked and in-place piles

Application of surcharge load over the soil domain introduces negative skin friction, and the same has been assessed through the numerical simulation. The shear stress profile, axial load and PWP distribution, effective radial stresses, contact status (i.e. slip or stick condition), settlement at the pile tip, and effective mean pressure obtained from the jacked and in-place cases, are compared in this section.

Shear stress and neutral plane

Figure 9 shows the shear stress along the depth of the pile for both jacked and in-place cases, after the end of the consolidation step. It can be noted that the jacked case shows mobilization of higher negative shear stress, i.e. higher negative skin friction, which is nearly double of that obtained from the in-place case. It can be further noticed that the pile installation type significantly influences the location of neutral plane. It can be observed from Fig. 9 that the neutral plane for the jacked case is located at approximately 17 m depth, which is about 3.5 m below the corresponding neutral plane for the in-place case. A general consensus is that stiffer the material at the pile base, deeper will be the location of the neutral plane (Fellenius, 1984; Lee and Ng, 2004). Hence, as it is expected that the pile jacking procedure would lead to an increase in the long-term stiffness of the soil beneath the pile as compared to the in-place case, the location of the neutral at larger depth for the former case is justified.

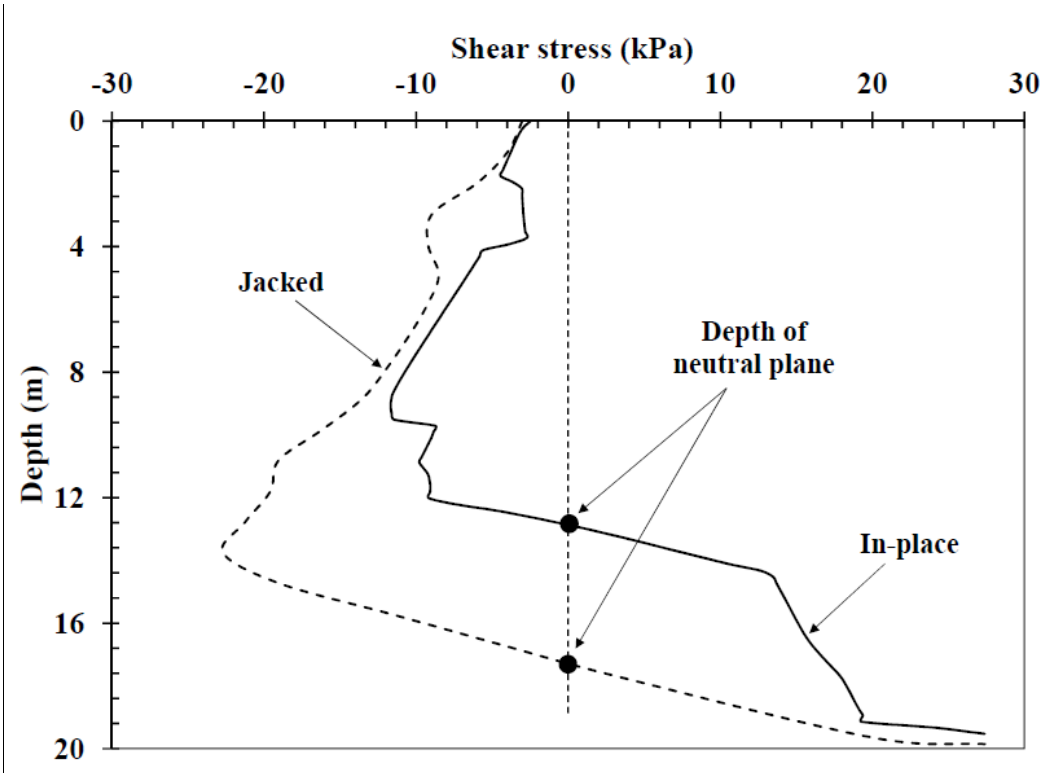

Fig. 9: Shear stress variation along the pile depth at the end of consolidation phase and location of the neutral planes.

507 ***Drag load and total pore-water pressure***

508 Figure 10 shows the variation of vertical drag load along with the depth of the pile. For
509 both the cases (jacked and in-place), increment in drag load has been obtained by integrating
510 the shear stress over the pile surface area. The drag load attains its maximum value at the
511 location of the corresponding neutral plane. For the jacked case, the maximum value of the
512 drag load is almost twice that achieved from the in-place case. The total PWP (POR) profile
513 obtained from the jacked and in-place cases, just after the application of surcharge load, has
514 been compared in Fig. 11 and a significant difference can be observed between the PWP
515 generated from these two methods. Larger PWP is observed at the pile tip for the jacked case
516 that is not evident for the latter one. This is owing to the jacking process that yields high-stress
517 concentration and subsequently higher accumulation of PWP near the pile tip.

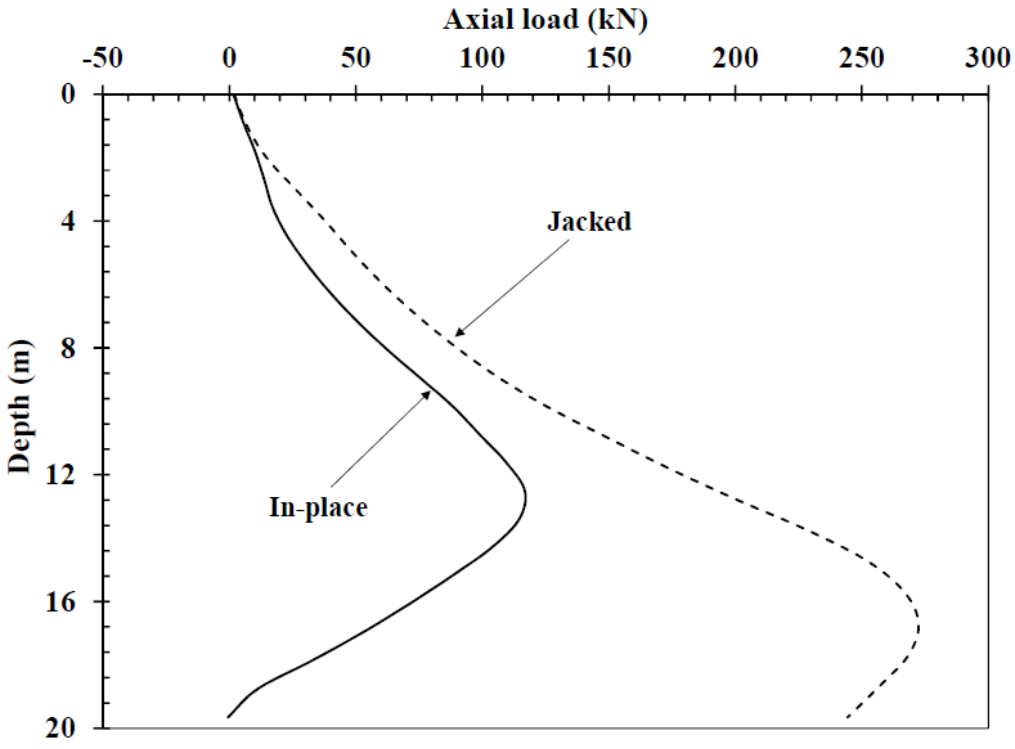

518

519 Fig. 10: Drag load variation at different depth along the pile at the end of consolidation phase.

520

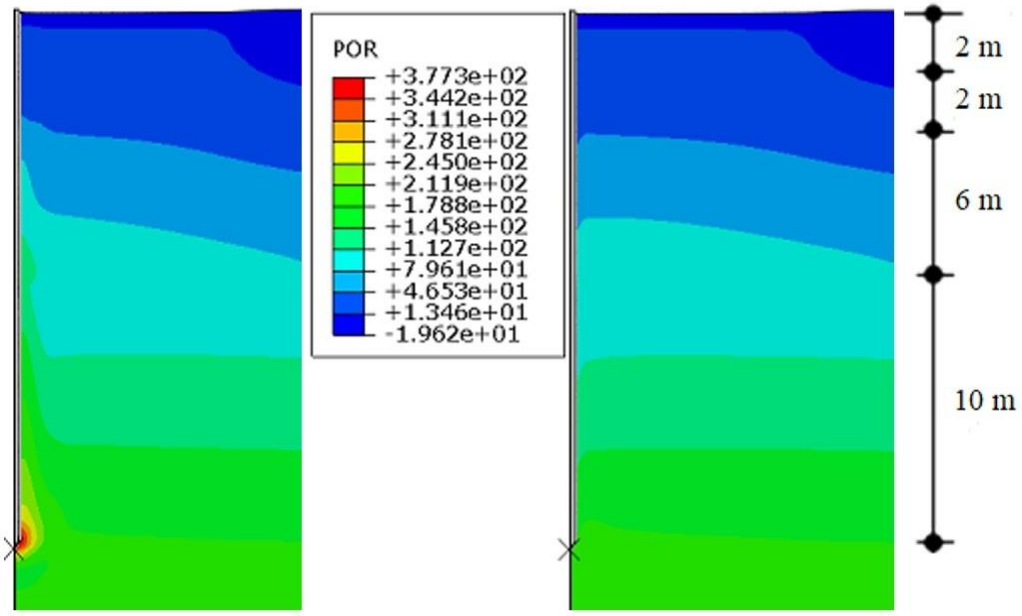

Fig. 11: Total pore-water pressure contour (POR, in kPa) around the pile for the (a) jacked case and (b) in-place case just after application of surcharge loading.

Effective radial stress

For jacked and in-place cases, Figure 12 shows the comparison of effective radial stress along the soil-pile interface at the end of the consolidation step. It can be observed that the jacked case exhibits higher effective radial stress along the interface and attains maximum value of 220 kPa near the pile base, while the maximum effective radial stress is 76 kPa for the in-place case. Figure 13 shows the evolution of effective radial stress for the jacked pile at various stages of the simulation. It can be observed that the effective radial stress remains unaltered during the surcharge loading phase and is almost similar to that in the initial condition. This implies that any possible increase in the total radial stress, attributed by the combined effect of pile jacking and subsequent surcharge loading, is almost completely borne by the generated excess pore-water pressure. It is justified considering the fact that the surrounding soil can still be undergoing undrained deformation during the jacking phase and the subsequent application of surcharge loading. This is also evident through the higher excess

pore-water pressure observed for the jacked pile at the commencement of the consolidation phase, as further discussed in a later section. Such higher excess pore-water pressures in the jacked case also indicate that in comparison to the in-place case, a larger total radial stress would be developed at the end of the surcharge loading phase. With the dissipation of excess pore-water pressure due to radial consolidation, the increased total radial stress is transferred as an increased effective radial stress at the soil-pile interface of the jacked pile. However, as the total radial stress is observed to be comparatively smaller for in-place case, the effective radial stresses transmitted are also smaller (Fig. 12). Hence, it can be concluded that the increased total radial stress in the jacked case induces a squeezing action that is not recognized for the in-place case, and the same is responsible for the generation of higher negative skin friction in jacked pile.

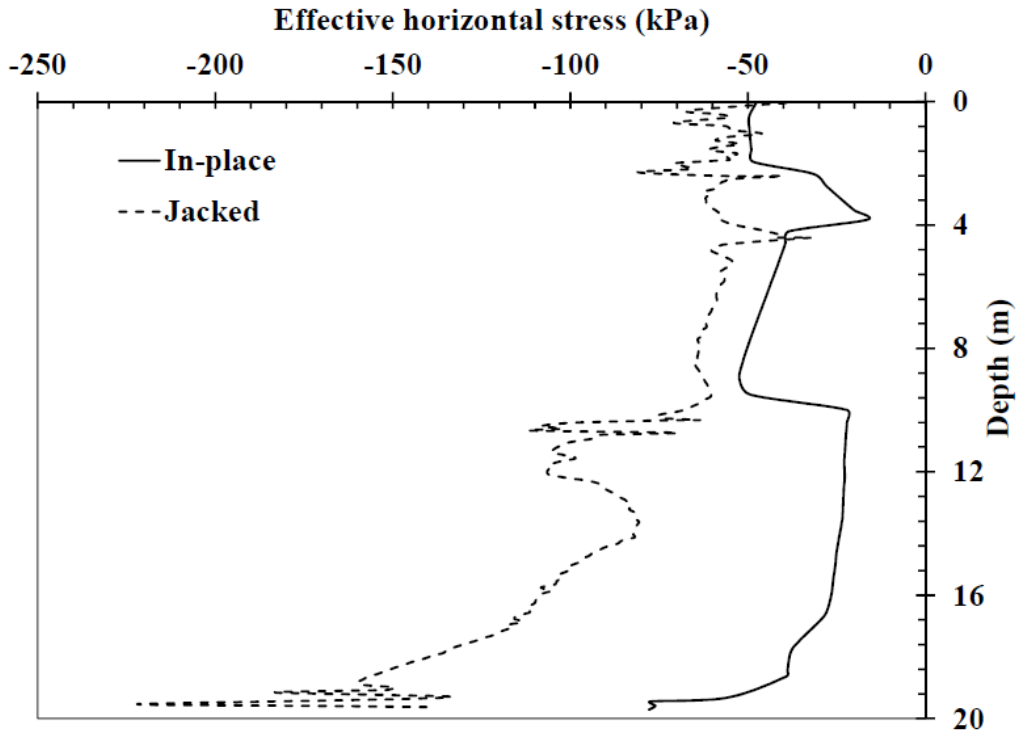

Fig. 12: Comparison of effective radial stress variation along the pile depth at the end of consolidation phase for the two different pile installation cases.

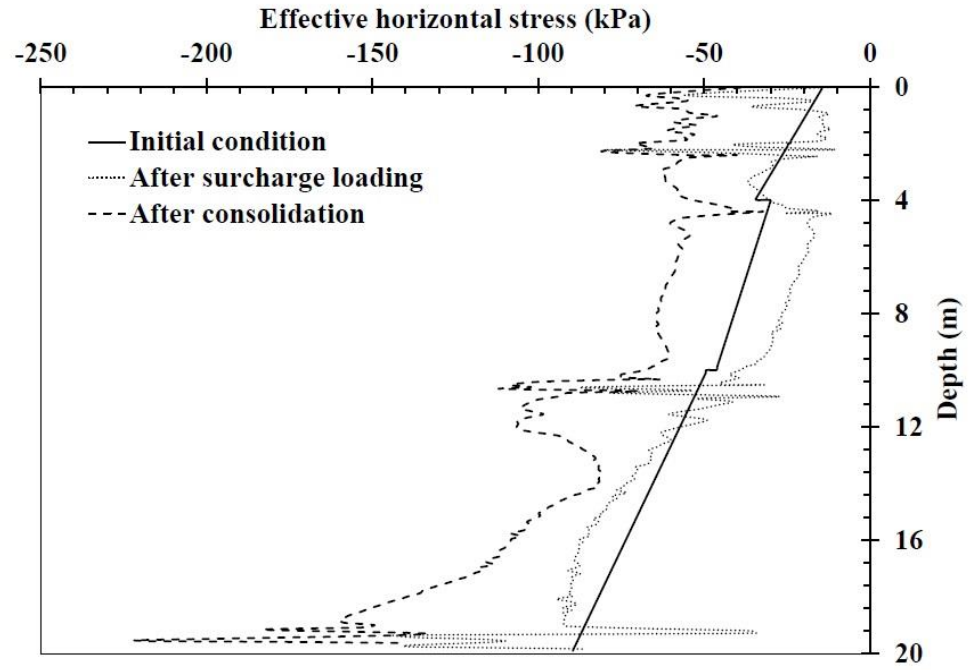

Fig. 13: Comparison of effective radial stress for the jacked case at various stages of simulation.

Contact status

Figure 14 shows the comparison of contact status at the end of consolidation phase, i.e. slip or stick condition, for the jacked and in-place cases. The contact status at the pile-soil interface has been indicated in the graph by two notations, i.e. '1' or '2', where '1' implies a slip condition and '2' implies a stick condition. A slip condition indicates that the plastic state has been reached at the soil-pile interface. For both the cases, soil-pile contact is observed to be in a state of slip for the upper part of the pile i.e. up to a penetration depth of approximately 10 m from the surface (Fig 14). This is due to the radial dissipation of the excess PWP, which leads to the excessive soil settlement near upper part of the pile. The plastic slip state has been noticed up to 14 m depth in the jacked case, which is almost 3-4 m deeper than the in-place case (Fig. 14). Pile penetration process attributes higher excess PWP in the adjacent soil than the in-place case, which upon radial consolidation, results in higher soil settlement. This might

be a reason for the deeper plastic slip state in the jacked case. The in-place case shows a slip condition again at the lower end of the pile. This is not due to the negative skin friction as the shear stress profile in this region is positive as shown in Fig. 9. This could be attributed to a higher settlement of the pile relative to the soil, which is further discussed in the next section.

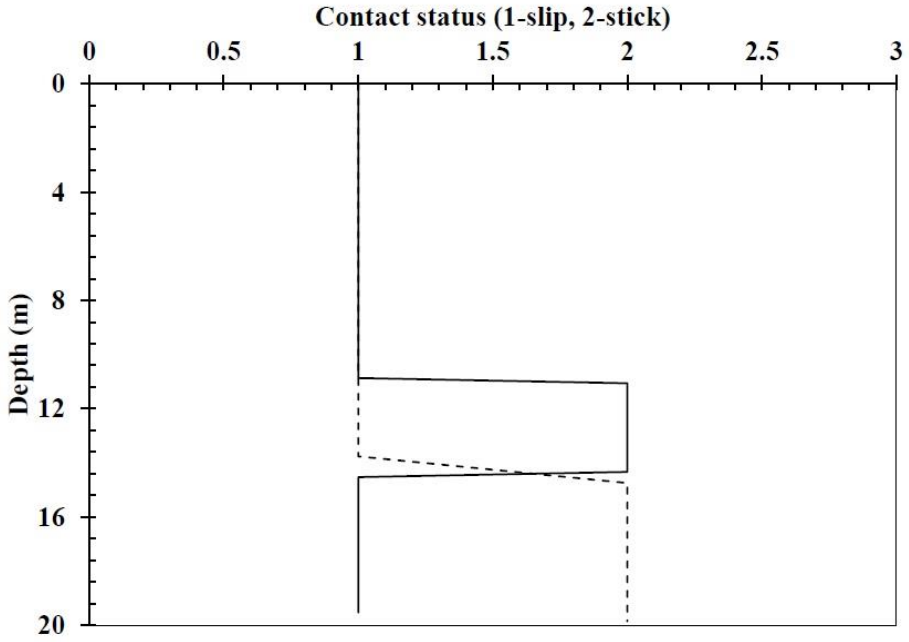

Fig. 14: Comparison of contact status, i.e. slip or stick, for the two different pile installation cases at the end of consolidation phase.

Settlement of pile

For both the jacked and in-place case during the consolidation process, Fig. 15 shows the settlement assessed at a node on the inclined face of the pile-tip half-cone. The settlement noted for the in-place case is in the order of 8 mm, while the settlement observed for the jacked case is about 1 mm (the negative sign implies a downward movement). Since the penetration process enhance the soil stiffness, low settlement is expected at the bottom of the pile for the jacked case. Due to the higher settlement observed at the tip of the in-place pile, the contact

583 status shows a slip condition again at the lower end of the pile (as is already pointed out at Fig.
584 14).

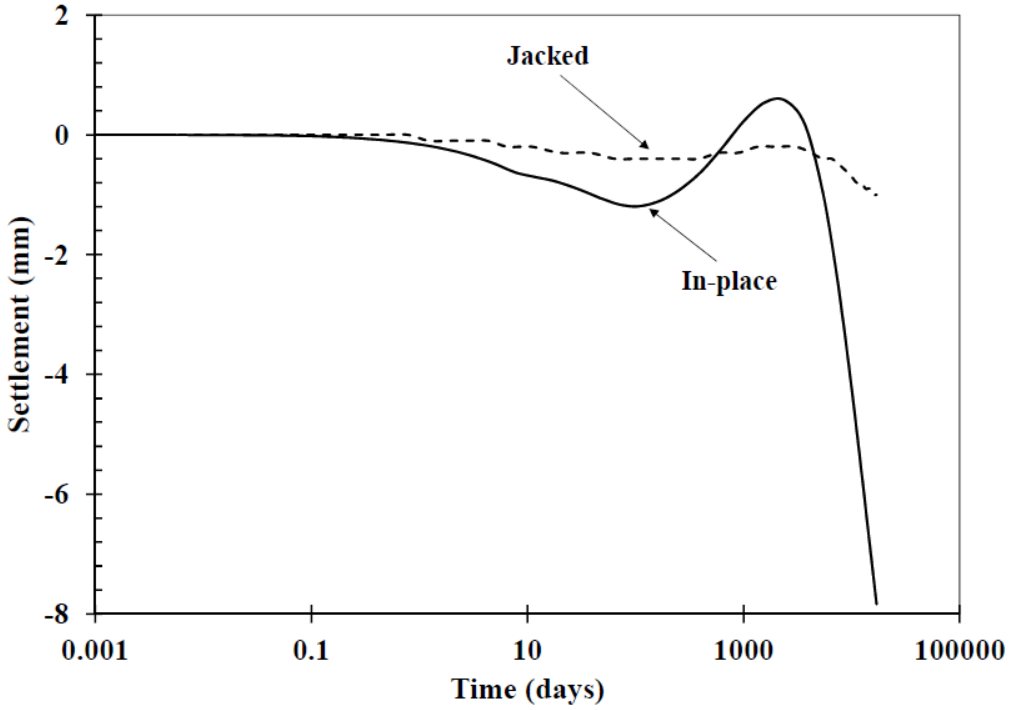

585

586 Fig. 15: Comparison of settlement of a node located at the pile base for jacked and in-place
587 case during the consolidation phase.

588

589 A slight upward movement of pile has been noticed for both the in-place and jacked
590 piles after few days of consolidation. This behaviour can be explained by observing the excess
591 PWP dissipation profile of each layer during the consolidation phase. In this regard, excess
592 PWP data has been extracted for points at a radial distance of 0.5 m from the soil-pile interface
593 and located at 1, 3, 7, 15 and 22 m depth from the ground surface, and are plotted against the
594 time as shown in Fig. 16 (a and b). The consolidation settlement of the soil depends upon the
595 excess PWP generated before commencing of the consolidation process, the length of drainage
596 path and permeability of the soil layers under consideration. Since the drainage boundary is
597 located at the level of the ground water table and the top soil layers have higher permeability

598 than the underlying layers, relatively rapid PWP dissipation has been noticed from the top soil
599 layers.

600 For both the in-place and jacked pile, immediately after the application of the surcharge
601 load on the ground surface, a rise in the excess PWP has been noticed at the 3, 7, 15, 20 and 22
602 m depths (Fig. 16). It is to be noted that the developed excess pore-water pressure is higher at
603 20 m depth in comparison to that developed at a greater depth of 22 m. However, for the jacked
604 pile, the magnitude of the excess pore-water pressure is significantly higher at 20 m depth due
605 to the penetration process itself. With the subsequent consolidation process, it is expected that
606 the developed excess pore-water pressure will get dissipated in all the directions. Due to the
607 presence of the drainage boundary at the level of water table (as shown in Fig. 1), a quicker
608 dissipation is induced in the upward direction. Additionally, due to the existence of a lower
609 excess pore-water pressure at the depth of 22 m developed at the initial stages, a dissipation
610 takes place in the downward direction as well. This is evident from the increase in the excess
611 pore-water pressure at 22 m depth from the 20^{th} day, for both the jacked and in-place case. This
612 increase in the excess pore-water pressure subsequently increases the total normal stress in the
613 soil layer just beneath the pile tip (i.e. the soil stratum at 20-22 m), thereby leading to a slight
614 upward displacement of the pile (as illustrated in Fig. 15). With the further dissipation of the
615 excess pore-water pressure from the least permeable layer due to the continued consolidation
616 process, a marked increase in pile settlement can be noticed approximately beyond 2500 days.
617 However, the overall pile settlement is observed to be smaller in the jacked case as compared
618 to the in-place case. This is attributed to the penetration process associated with the former one,
619 which resulted in an overall higher mean effective stress (as shown in Fig. 17a) and increased
620 stiffness at the bottom of the jacked pile.

621

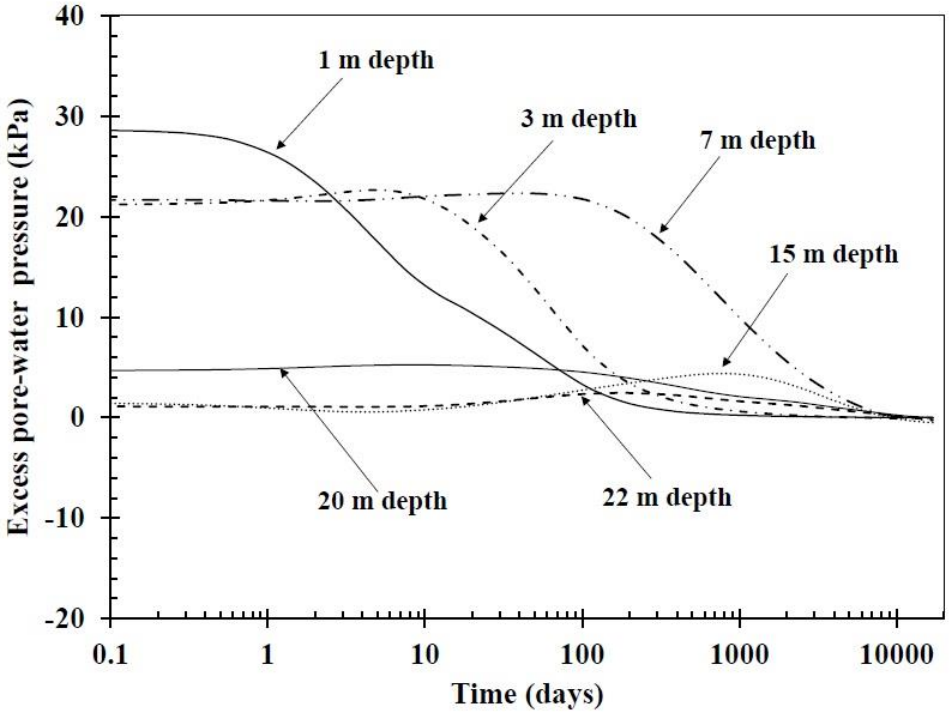

(a)

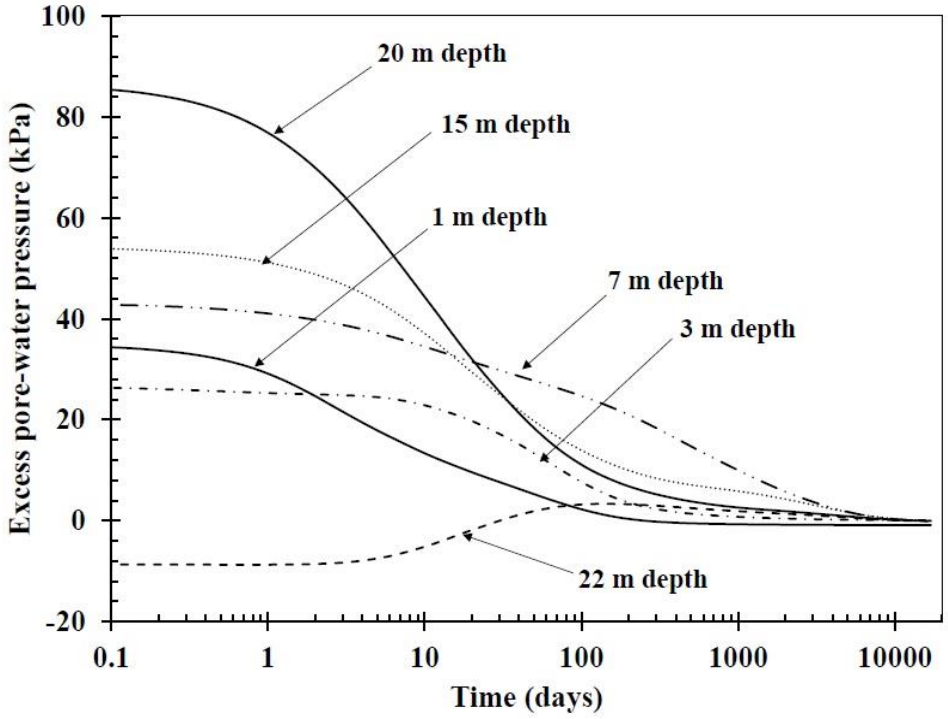

(b)

Fig. 16: Excess pore-water pressure dissipation at 0.5 m radial distance from the soil-pile interface and at various depths for (a) in-place and (b) jacked case during the consolidation phase.

629 ***Effective mean stress***

630 The development of effective mean stress throughout the consolidation process in an
631 element just below the pile tip has been compared in Fig. 17a. The effective mean stress for
632 the in-place case remains fairly constant during the consolidation process; whereas, a stark
633 increment of about 50% has been observed for the jacked case. The excess PWP dissipation
634 curve has also been plotted for a node adjacent to the pile tip (Fig. 17b) and a significant
635 reduction in the excess PWP has been noticed for the jacked case. Hence, it can be concluded
636 that the process of pile jacking results in an increase in the total mean stress near the pile tip,
637 which leads to a significant increase in the effective mean stress of the soil due to the dissipation
638 of PWP during the consolidation phase. The same trend can be noticed from Fig. 18, which
639 shows a comparison of spatial distribution of effective mean stress (S) for both the pile
640 installation cases at the end of consolidation step. Such increased effective mean stress for the
641 jacked case eventually leads to an enhanced stiffness and further reduction in the pile settlement
642 as discussed in the previous section. It can be noticed that for the jacked case, there exists a
643 small region near the pile base, which experiences a decrease in effective mean stress. This
644 might be due to the formation of an expansion zone at some depth beneath the pile tip (as in
645 Fig. 18a), as has been also noticed in the simulations of pile penetration by the past researchers
646 (Sheng *et al*., 2005).

647

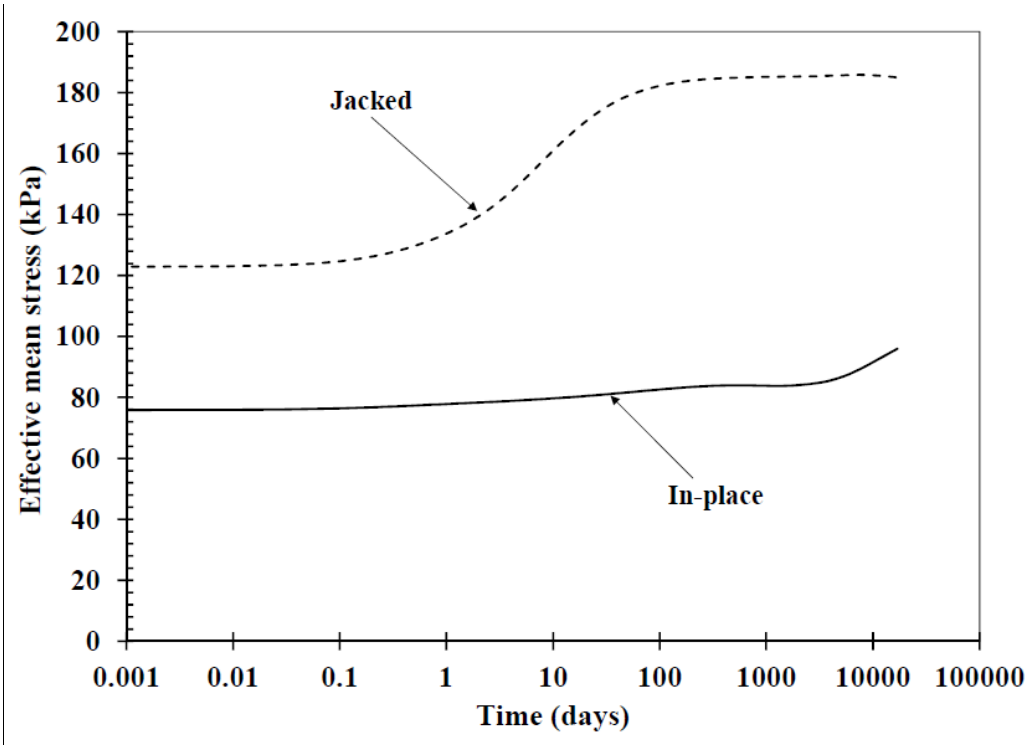

(a)

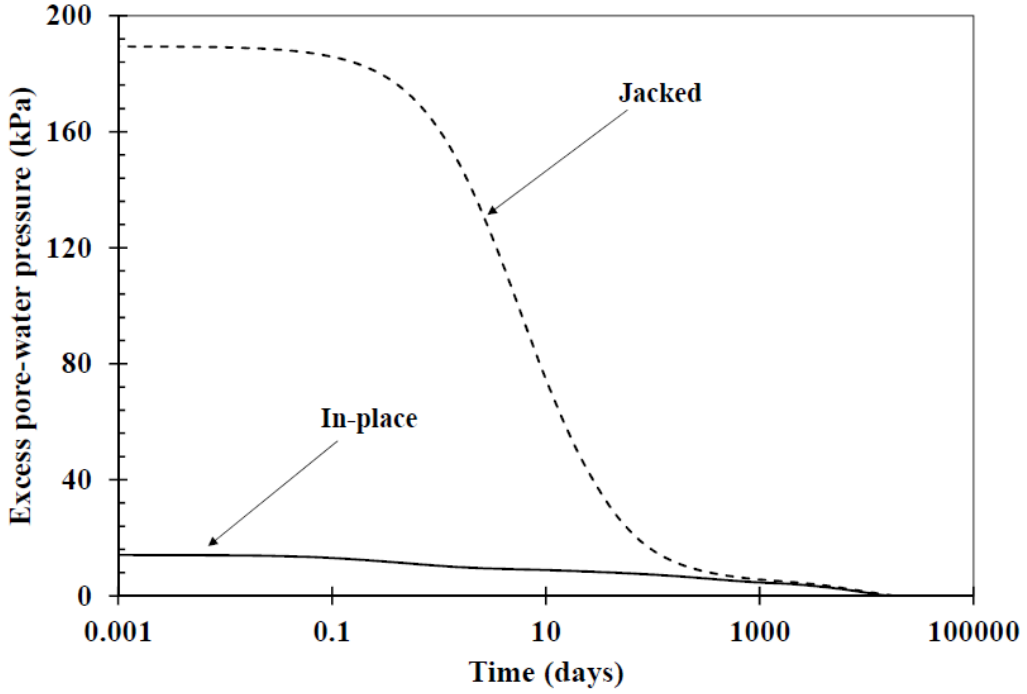

(b)

Fig. 17: Comparison of (a) effective mean stress and (b) excess pore-water pressure developed beneath the pile base for jacked and in-place case during the consolidation phase.

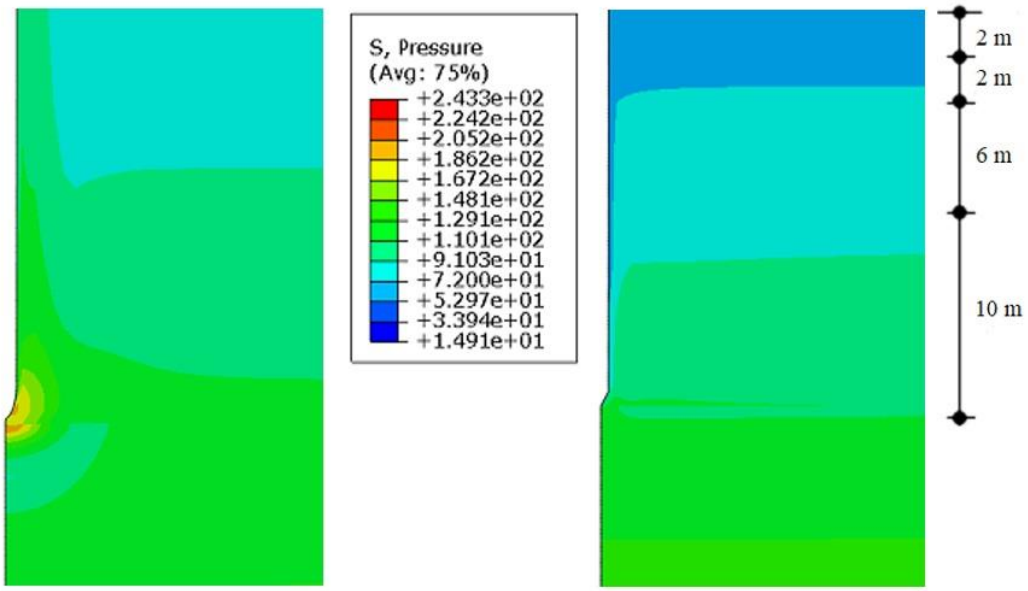

Fig. 18: Comparison of effective mean stress (S, in kPa) at the pile base for the (a) jacked and (b) in-place case at the end of consolidation phase.

Conclusions

The present study attempts to explore the role of pile installation schemes on the generation of negative skin friction by performing numerical simulations considering two different cases, first an in-situ installation scheme and the second one addressing the jacking process at a constant penetration rate. The pile jacking process has been simulated by an updated Lagrangian approach in a 2D axisymmetric finite element framework and the nonlinear pile-soil interaction has been modelled through the penalty stiffness method. In order to achieve an effective pile penetration simulation within a large-deformation based finite element simulation framework, a series of pre-processing steps prior to the actual analysis is necessary. These includes placement of a rigid thin solid tube to enable axisymmetric boundary condition while pile jacking, selection of cone angle, contact stiffness parameter and optimal mesh discretization. A detailed study of the influence of these parameters has been carried out and their optimum values are identified and further employed in the simulation. The adopted

672 simulation approach has been validated against the field study reported by Indraratna *et al.*
673 (1990) in terms of the generated excess pore-water pressure during the penetration process and
674 its subsequent dissipation with time.

675 To compare the effect of pile installation schemes on the eventual development of
676 negative skin friction, this paper considers surcharge loading applied only on the surrounding
677 soft clay and no such surcharge load is applied on the pile itself. The two most important
678 differences in pile response for the two installation procedures, which emerge from the
679 numerical study, are the axial load response and the pile-tip settlement response. Dissipation
680 of higher induced excess pore water pressures during pile jacking and the comparatively lower
681 location of the neutral plane lead to higher negative stresses acting along a larger
682 circumferential area of the pile inducing a larger axial load for the jacked case as compared to
683 the in-place case. In this study, the maximum axial load was recognized to be approximately
684 2.5 times larger when the jacking process was simulated as compared to the in-place case. This
685 indicates that careful considerations have to be made in terms of the structural strength or
686 capacity of the pile, especially after the additive surcharge load is applied and there is a
687 considerable chance that in-place simulations might underestimate the total axial load acting
688 on a jacked pile.

689 Jacking of the pile followed by consolidation is observed to produce much larger mean
690 effective stresses in the soil at the pile base as compared to the in-place simulations. This
691 indicates that the actual contribution of base resistance to the final bearing capacity of the pile
692 is higher than that indicated by in-place simulations. This potential improvement in soil
693 strength near the pile base due to jacking is completely overlooked by in-place simulations
694 which might produce higher estimates of expected settlement leading to overly conservative
695 designs.

696 **Acknowledgement**

697 The authors would like to thank SERB (Grant no. ECR/2018/002141) for the financial support
698 towards carrying out part of this research.

699

700 **References**

701 Abaqus User's Manual, 2018, version 6.14, Dassault Systèmes.

702 Aubram, D., Rackwitz, F., Wriggers, P., 2015. An ALE method for penetration into sand
703 utilizing optimization-based mesh motion. *Computers and Geotechnics*, 65, 241–249.
704 https://doi.org/10.1016/j.compgeo.2014.12.012

705 Bathe, K.J., 1996. Finite Element Procedures. PHI Learning Private Limited, India.

706 Belytschko, T., Liu, W.K., Moran, B., 2001. Nonlinear Finite Elements for Continua and
707 Structures. *John Wiley and Sons, Inc.*, USA.

708 Blanchet, R., Tavenas, F.A., Garneau, R., 1980. Behavior of friction piles in soft sensitive
709 clays. *Canadian Geotechnical Journal*, 17, 203-224. https://doi.org/10.1139/t80-023

710 Cao, W., Chen, Y., Wolfe, W.E., 2014. New load transfer hyperbolic model for pile-soil
711 interface and negative skin friction on single piles embedded in soft soils. *International*
712 *Journal of Geomechanics, ASCE*, 14(1), 92-100. https://doi.org/10.1061/(ASCE)GM.1943-
713 5622.0000289

714 Carter, J.P., Randolph, M.F., Wroth, C.P., 1979. Stress and pore pressure changes in clay
715 during and after the expansion of a cylindrical cavity. *International Journal for Numerical*
716 *and Analytical Methods in Geomechanics*, 3(4), 305-322.
717 https://doi.org/10.1002/nag.1610030402

718 Ceccato, F., Beuth, L., Simonini, P., 2016. Analysis of piezocone penetration under different
719 drainage conditions with the two-phase material point method. *Journal of Geotechnical and*
720 *Geoenvironmental Engineering ASCE*, 142(12), 04016066.
721 https://doi.org/10.1061/(ASCE)GT.1943-5606.0001550

722 Ceccato, F., Simonini, P., 2017. Numerical study of partially drained penetration and pore
723 pressure dissipation in piezocone test. *Acta Geotechnica*, 12(1), 195-209.
724 https://doi.org/10.1007/s11440-016-0448-6

725 Comodromos, E.M., Bareka, S.V., 2005. Evaluation of negative skin friction effects in the pile
726 foundations using 3D nonlinear analysis. *Computers and Geotechnics*, 32, 210-221.
727 https://doi.org/10.1016/j.compgeo.2005.01.006

728 Ebrahimipour, A., Eslami, A., 2024. Analytical study of piles behavior for marine challenging
729 substructures. *Ocean Engineering* 292(116514), 1-12. https://doi.org/10.1016/
730 j.oceaneng.2023.116514

731 Ekanayake, S.D., Liyanapathirana, D.S., Leo, C.J., 2013. Influence zone around a closed-ended
732 pile during vibratory driving. *Soil Dynamics and Earthquake Engineering*, 53, 26-36.
733 https://doi.org/10.1016/j.soildyn.2013.06.005

734 Fall, M., Gao, Z., Ndiaye, B.C., 2021. Driven pile effects on nearby cylindrical and semi-
735 tapered pile in sandy clay. *Applied Science, MDPI*, 11, 2919.
736 https://doi.org/10.3390/app11072919

737 Fan, S., Bienen, B., Randolph, M.F., 2018. Stability and efficiency studies in the numerical
738 simulation of cone penetration in sand. *Géotechnique Letters*, 8, 13–18.
739 https://doi.org/10.1680/jgele.17.00105

740 Fan, S., Bienen, B., Randolph, M.F., 2021. Effects of monopile installation on subsequent
741 lateral response in sand. I: Pile installation. *Journal of Geotechnical and Geoenvironmental*
742 *Engineering, ASCE*, 147(5), 04021021. https://doi.org/10.1061/(ASCE)GT.1943-
743 5606.0002467

744 Fellenius, B.H., 1984. Negative skin friction and settlement of piles. *Second International*
745 *Seminar on Pile Foundations*, Singapore, 1-12.

746 Fellenius, B.H., 1972. Down-drag on piles in clay due to negative skin friction. *Canadian*
747 *Geotechnical Journal*, 9(4), 323-337. https://doi.org/10.1139/t72-037

748 Fischer, K.A., Sheng, D., Abbo, A.J., 2007. Modeling of pile installation using contact
749 mechanics and quadratic elements. *Computers and Geotechnics*, 34, 449-461.
750 https://doi.org/10.1016/j.compgeo.2007.01.003

751 Ghosh Dastider, A., Chatterjee, S., Basu, P., 2022. Advancement in estimation of undrained
752 shear strength through fall cone tests. *Journal of Geotechnical and Geoenvironmental*
753 *Engineering, ASCE*, 147(7), 1-10. https://doi.org/10.1061/(ASCE)GT.1943-5606.0002535

754 Hamann, T., Qiu, G., Grabe, J., 2015. Application of a coupled Eulerian-Lagrangian approach
755 on pile installation problems under partially drained conditions. *Computers and*
756 *Geotechnics*, 63, 279-290. https://doi.org/10.1016/j.compgeo.2014.10.006

757 Henke, S., 2010. Influence of pile installation on adjacent structures. *International Journal for*
758 *Numerical and Analytical Methods in Geomechanics*, 34(11), 191–210.
759 https://doi.org/10.1002/nag.859

760 Hosseini, M.A., Rayhani, M. 2017. Evolution of pile shaft capacity over time in marine soils.
761 *International Journal of Geo-Engineering*, 8(12), 1-15. https://doi.org/10.1186/s40703-
762 017-0049-8

763 Hwang, J.H., Liang, N., Chen, C.H., 2001. Ground response during pile driving. *Journal of*
764 *Geotechnical and Geoenvironmental Engineering, ASCE*, 127(11), 939-949.
765 https://doi.org/10.1061/(ASCE)1090-0241(2001)127:11(939)

766 Igoe, D., Gavin, K., O'Kelly, B. 2013. An investigation into the use of push-in pile foundations
767 by the offshore wind sector. *International Journal for Environmental Studies*, 70(5), 777-
768 791. http://dx.doi.org/10.1080/00207233.2013.798496

769 Indraratna, B., Balasubramaniam, A.S., Phamvan, P., Wong Y.K., 1992. Development of
770 negative skin friction on driven piles in soft Bangkok clay. *Canadian Geotechnical Journal*,
771 29(3), 393–404. https://doi.org/10.1139/t92-044

772 Jeong, S., Ko, J., Lee, C., Kim, J. 2014. A response of single piles in marine deposits to negative
773 skin friction from long-term field monitoring. *Marine Georesources and Geotechnology*,
774 32, 239-263. http://dx.doi.org/10.1080/1064119X.2012.735344

Jeong, S., Lee, J., Lee, C.J., 2004. Slip effect at the pile–soil interface on dragload. *Computers and Geotechnics*, 31(2), 115–126. https://doi.org/10.1016/j.compgeo.2004.01.009

Kouretzis, G.P., Sheng, D., Wang, D., 2014. Numerical simulation of cone penetration testing using a new critical state constitutive model for sand. *Computers and Geotechnics*, 56, 50–60. https://doi.org/10.1016/j.compgeo.2013.11.002

Lam, S.Y., Charles, Ng, W.W., Leung, C.F., Chan, S.H., 2009. Centrifuge and numerical modelling of axial load effects on pile in consolidating ground. *Canadian Geotechnical Journal*, 46, 10-24. https://doi.org/10.1139/T08-095

Lee, C.J., Ng, C.W.W., 2004. Development of downdrag on piles and pile groups in consolidating soil. *Journal of Geotechnical and Geoenvironmental Engineering, ASCE*, 130(9), 905-914. https://doi.org/10.1061/(ASCE)1090-0241(2004)130:9(905)

Lee, C.J., Bolton, M.D., Al-Tabaa, A., 2001. Recent findings on negative skin friction in piles and pile groups in consolidating ground. *5th International Conference on Deep Foundation Practice Incorporating Piletalk*, Singapore, 273-280.

Lee, P.T., Tan, Y.C., Bok, J.G. 2019. Design and construction of driven piles over soft marine clay. *Proceedings of the 16th Asian Regional Conference on Soil Mechanics and Geotechnical Engineering*, Taipei, Taiwan, 1-4.

Leung, C.F., Liao, B.K., Chow, Y.K., Shen, R.F., Kog, Y.C. 2004. Behavior of pile subject to negative skin friction and axial load. *Soils and Foundations*, 44(6), 17-26. https://doi.org/10.3208/sandf.44.6_17

Liu, J., Gao, H., Liu, H., 2012. Finite element analyses of negative skin friction on a single pile. *Acta Geotechnica*, 7, 239-252. https://doi.org/10.1007/s11440-012-0163-x

Liu, Y.-H., Yang, P., Xue, S., Pan, Y.-F., 2020. Influence of dredger fill self-consolidation on development of negative skin friction of piles. *Arabian Journal of Geosciences* 13, 75-1-8. https://doi.org/10.1007/s12517-020-05739-3

Liyanapathirana, D.S., 2009. Arbitrary Lagrangian Eulerian based finite element analysis of cone penetration in soft clay. *Computers and Geotechnics*, 36, 851–860. https://doi.org/10.1016/j.compgeo.2009.01.006

Mabsout, M.E., Tassoulas, J.A., 1994. A finite element model for the simulation of pile driving. *International Journal for Numerical Methods in Engineering*, 37, 257–78. https://doi.org/10.1002/nme.1620370206

Monforte, L., Arroyo, M., Carbonell, J.M., Gens, A., 2018. Coupled effective stress analysis of insertion problems in geotechnics with the Particle Finite Element Method. *Computers and Geotechnics*, 101, 114-129. https://doi.org/10.1016/j.compgeo.2018.04.002

Poulos H.G., Davis E.H., 1980. Pile Foundation Analysis and Design. John Wiley and Sons, New York, USA.

Pucker, T., Grabe, J., 2012. Numerical simulation of the installation process of full displacement piles. *Computers and Geotechnics*, 45, 93–106. https://doi.org/10.1016/j.compgeo.2012.05.006

Qiu, G, Henke, S., Grabe, J., 2011. Application of a coupled Eulerian–Lagrangian approach on geomechanical problems involving large deformations. *Computers and Geotechnics*, 38(1), 30–39. https://doi.org/10.1016/j.compgeo.2010.09.002

Randolph, M.F., Carter, J.P., Wroth, C.P., 1979. Driven piles in clay-the effects of installation and subsequent consolidation. *Geotechnique*, 29(4), 361-393. https://doi.org/10.1680/geot.1979.29.4.361

Randolph, M.F., Wroth, C.P., 1979. An analytical solution for the consolidation around a driven pile. *International Journal for Numerical and Analytical Methods in Geomechanics*, 3(3), 217-229. https://doi.org/10.1002/nag.1610030302

Sabetamal, H., Nazem, M., Carter, J., Sloan, S., 2014. Large deformation dynamic analysis of saturated porous media with applications to penetration problems. *Computers and Geotechnics*, 55, 117–131. https://doi.org/10.1016/j.compgeo.2013.08.005

Sahu, S.K., Kumar, V., Dutta, S.C., Sarkar, R., Bhattacharya, S., Debnath, P., 2020. Structural safety of offshore wind turbines: Present state of knowledge and future challenges. *Ocean Engineering* 309(118383), 1-18. https://doi.org/10.1016/j.oceaneng.2024.118383

829 Shen, K., Wang, K., Yao, J., Yu, J., 2022. Numerical investigation on behavior of compressive
830 piles in coastal tidal flat with fill. *Journal of Marine Science and Engineering* 10, 1742-1-
831 13. https://doi.org/10.3390/jmse10111742

832 Sheng, D., Cui, L., Ansari, Y., 2013. Interpretation of cone factor in undrained soils via full-
833 penetration finite-element analysis. *International Journal of Geomechanics, ASCE*, 13(6),
834 745-753. https://doi.org/10.1061/(ASCE)GM.1943-5622.0000279

835 Sheng, D., Eigenbrod, K.D., Wriggers, P., 2005. Finite element analysis of pile installation
836 using large-slip frictional contact. *Computers and Geotechnics*, 32, 17-26.
837 https://doi.org/10.1016/j.compgeo.2004.10.004

838 Sheng, D., Nazem, M., Carter, J. P., 2009. Some computational aspects for solving deep
839 penetration problem in geomechanics. *Computational Mechanics*, 44(4), 549–561.
840 https://doi.org/10.1007/s00466-009-0391-6

841 Sheng, D., Wriggers, P., Sloan, S.W., 2006. Improved numerical algorithms for frictional
842 contact in pile penetration analysis. *Computers and Geotechnics*, 33, 341-354.
843 https://doi.org/10.1016/j.compgeo.2006.06.001

844 Simo, J. C., Meschke, G., 1993. A new class of algorithms for classical plasticity extended to
845 finite strains: Application to geomaterials. *Computational Mechanics*, 11(4), 253–278.
846 https://doi.org/10.1007/BF00371865

847 Tho, K.K, Leung, C.F., Chow, Y.K., Swaddiwudhipong, S., 2012. Eulerian finite element
848 technique for analysis of jack-up spudcan penetration. *International Journal of*
849 *Geomechanics, ASCE*, 12(1), 64–73. https://doi.org/10.1061/(ASCE)GM.1943-
850 5622.0000111

851 Tolooiyan, A., Gavin, K., 2011. Modelling the cone penetration test in sand using cavity
852 expansion and arbitrary Lagrangian Eulerian finite element methods. *Computers and*
853 *Geotechnics*, 38(4), 482-490. https://doi.org/10.1016/j.compgeo.2011.02.012

854 Walker, J., Yu, H., 2006. Adaptive finite element analysis of cone penetration in clay. *Acta*
855 *Geotechnica*, 1(1), 43–57. https://doi.org/10.1007/s11440-006-0005-9

Wang, D., Bienen, B., Nazem, M., Tian, Y.H., Zheng, J.B., Pucker, T., Randolph, M.F., 2015. Large deformation finite element analyses in geotechnical engineering. *Computers and Geotechnics*, 65, 104–114. https://doi.org/10.1016/j.compgeo.2014.12.005

Wang, J., Wu, X., Qin, W., Chang, K., 2023. Negative skin friction of piles installed in dredged slurry after being reinforced by the vacuum preloading method. *Acta Geotechnica* 18, 6159-6174. https://doi.org/10.1007/s11440-023-01998-y

Wriggers, P., 2006. Computational Contact Mechanics. Springer-Verlag, Berlin, Germany.

Wu, W., Wang, Z., Zhang, Y., El Naggar, M.H., Wu, T., Wen, M. (2023). Semi-analytical solution for negative skin friction development on deep foundations in coastal reclamation areas. *International Journal of Mechanical Sciences* 241(107981), 1-21. https://doi.org/10.1016/j.ijmecsci.2022.107981

Yi, J.T., Goh, S.H., Lee, F.H., Randolph, M.F., 2012. A numerical study of cone penetration in fine grained soils allowing for consolidation effects. *Geotechnique*, 62(8), 707-719. https://doi.org/10.1680/geot.8.P.155

Yuan, W.H., Zhang, W., Dai, B., Wang, Y., 2019. Application of the particle finite element method for large deformation consolidation analysis. *Engineering Computations*, 36(9), 3138-3163. https://doi.org/10.1108/EC-09-2018-0407

Zhao, H., Yang, X., Zheng, H., Yan, X., Lian J., 2023. Coupled Eulerian-Lagrangian finite element analysis of penetration processes in silty clay for bucket foundation. *Ships and Offshore Structures*, 18(12), 1701-1712. https://doi.org/10.1080/17445302.2022.2140521